FIGURES

Fig. 1. Posterior pole region of live cleavage embryos photographed with Nomarski optics. Wild-type (A), N441 (B), N26 (C) and par (D) embryos are shown. Arrowhead indicates the space between egg plasma membrane and vitelline membrane. Bar represents 50 μm.

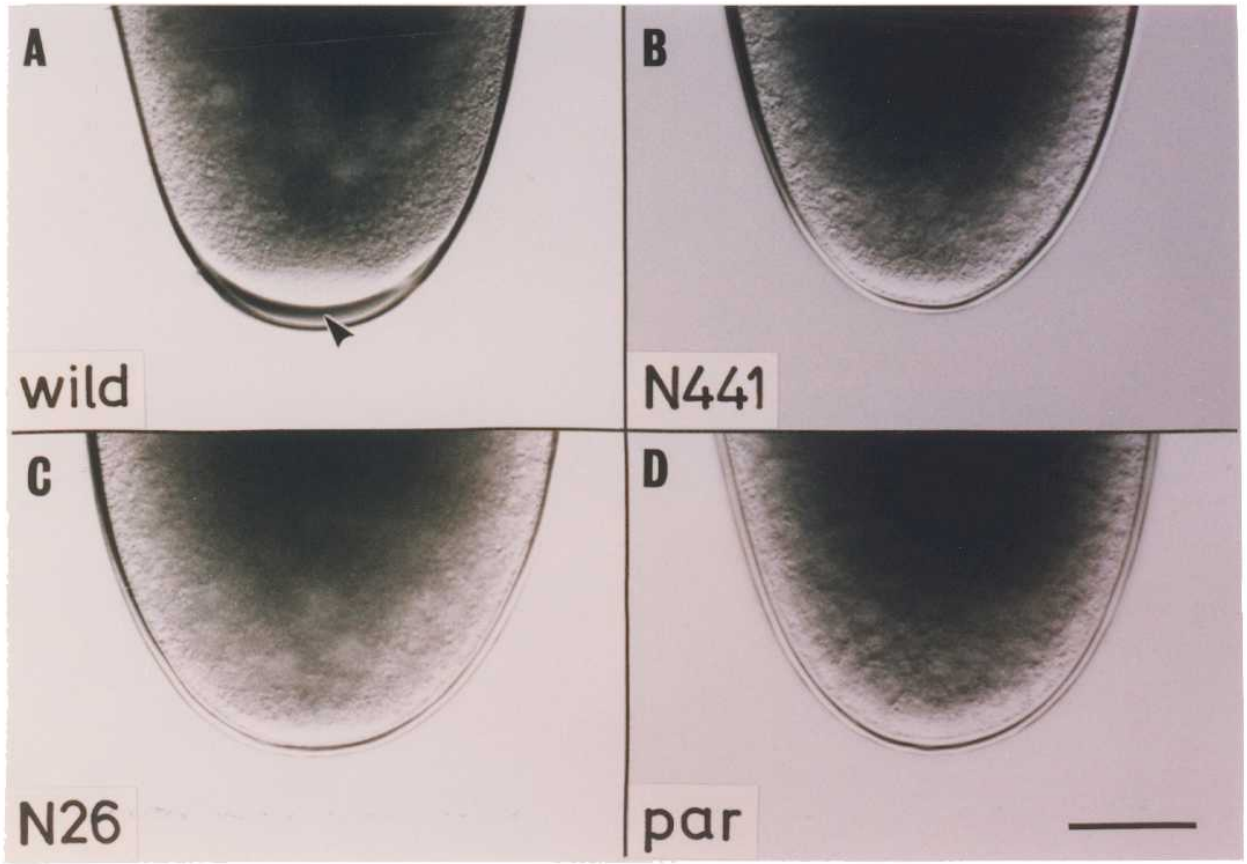
A
wild
B
N441
C
N26
D
par

Fig. 2. Whole mount cycle-8 embryos from mothers raised under a restrictive condition. Nuclei were stained with basic fuchsin. Wild-type (A), N441 (B), N26 (C) and par (D) embryos are shown. Anterior poles are to the top. Arrowheads indicate the most anterior and the most posterior nuclei in each embryo. Bar represents 50 μm.

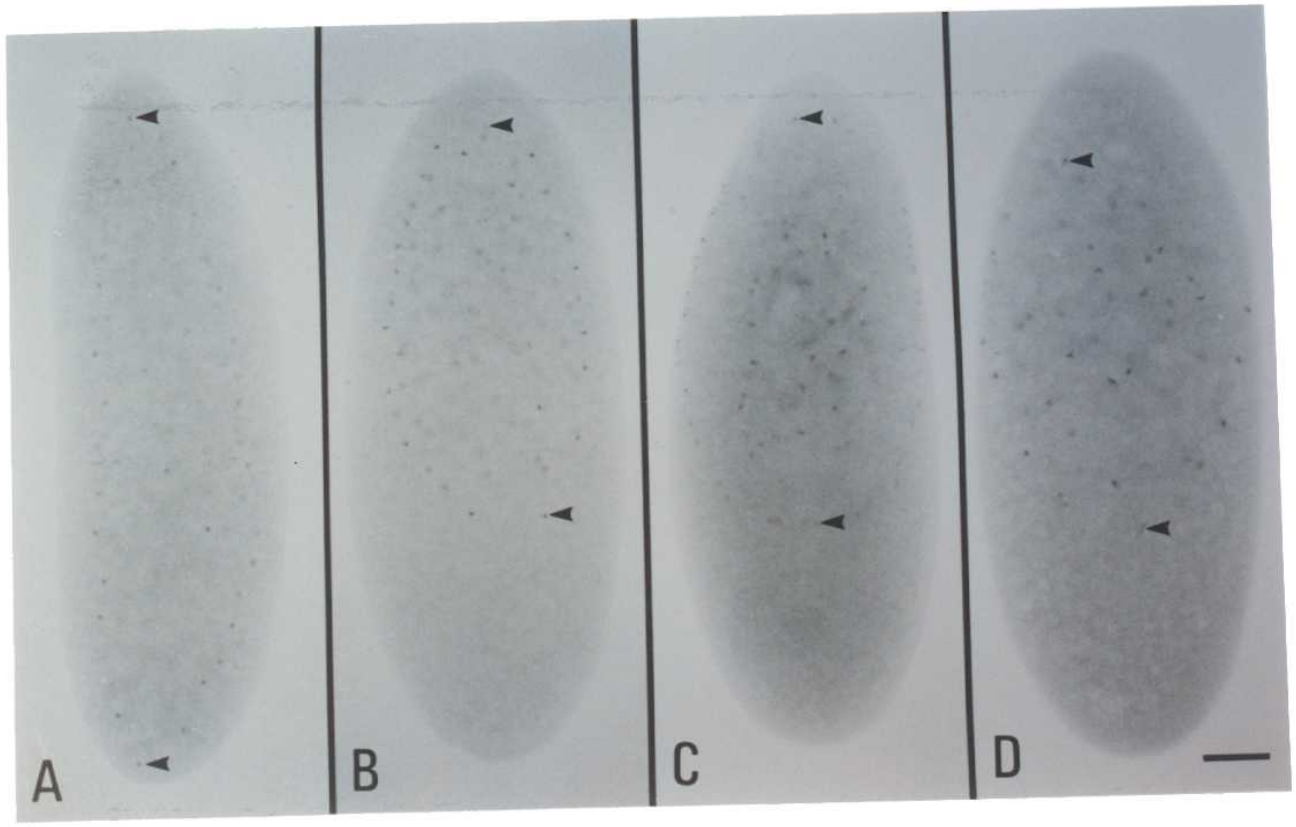
A
B
C
D

Fig. 3. Mitotic waves in N441 embryos. (A), a cycle-8 embryo from a mother raised under a permissive condition (note that the nuclei close to the posterior pole indicated by arrowheads are in anaphase to telophase in ahead of others); (B), a syncytial blastoderm embryo from a mother raised under a restrictive condition. Nuclei were stained with DAPI. Anterior poles are to the top-left corner. Bar represents 100 μm.

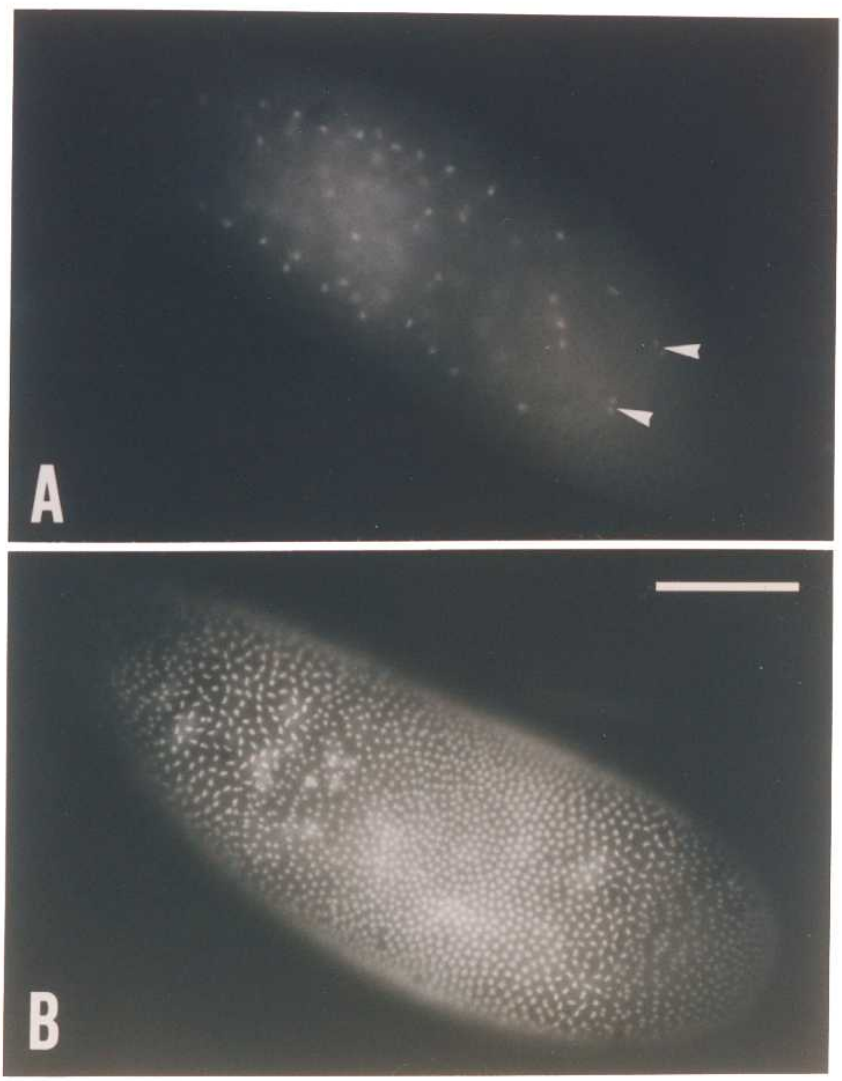
A
B

Fig. 4. Change in the range of nuclear distribution along the anteroposterior axis throughout the cleavage stages in the embryos from homozygous mothers raised under a restrictive condition. The positions of the most anterior and the most posterior nuclei presented in Table 1 are visualized in this figure. The shaded area represents the range of nuclear distribution in the wild type. The ranges of nuclear distribution in mutant embryos are represented by the area limited by solid lines for N441, by broken lines for N26 and by dot-broken lines for par. 0% egg length indicates the posterior pole. Vertical bars represent standard errors.

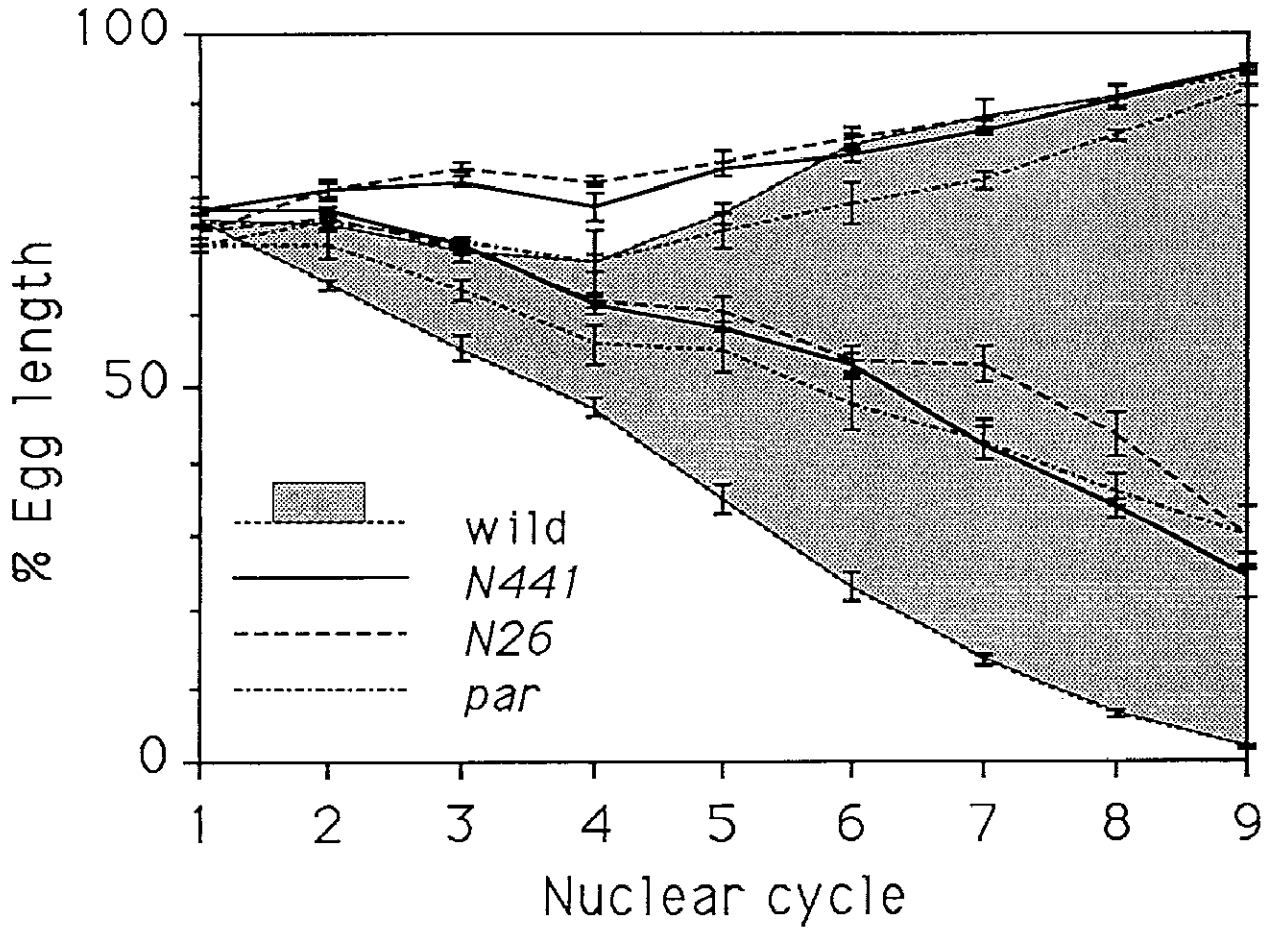
100
50
0
% Egg length
wild
N441
N26
par
1
2
3
4
5
6
7
8
9
Nuclear cycle

Fig. 5. Change in the range of nuclear distribution along the anteroposterior axis throughout the cleavage stages in the embryos from homozygous mutant mothers raised under a permissive condition. The positions of the most anterior and the most posterior nuclei presented in Table 2 are visualized in this figure. Nuclear distribution is represented by the area limited by solid lines for N441, by broken lines for N26 and by dot-broken lines for par. The shaded area represents the range of nuclear distribution in the wild-type embryos from mothers raised at 25°C. 0% egg length indicates the posterior pole. Vertical bars represent standard errors.

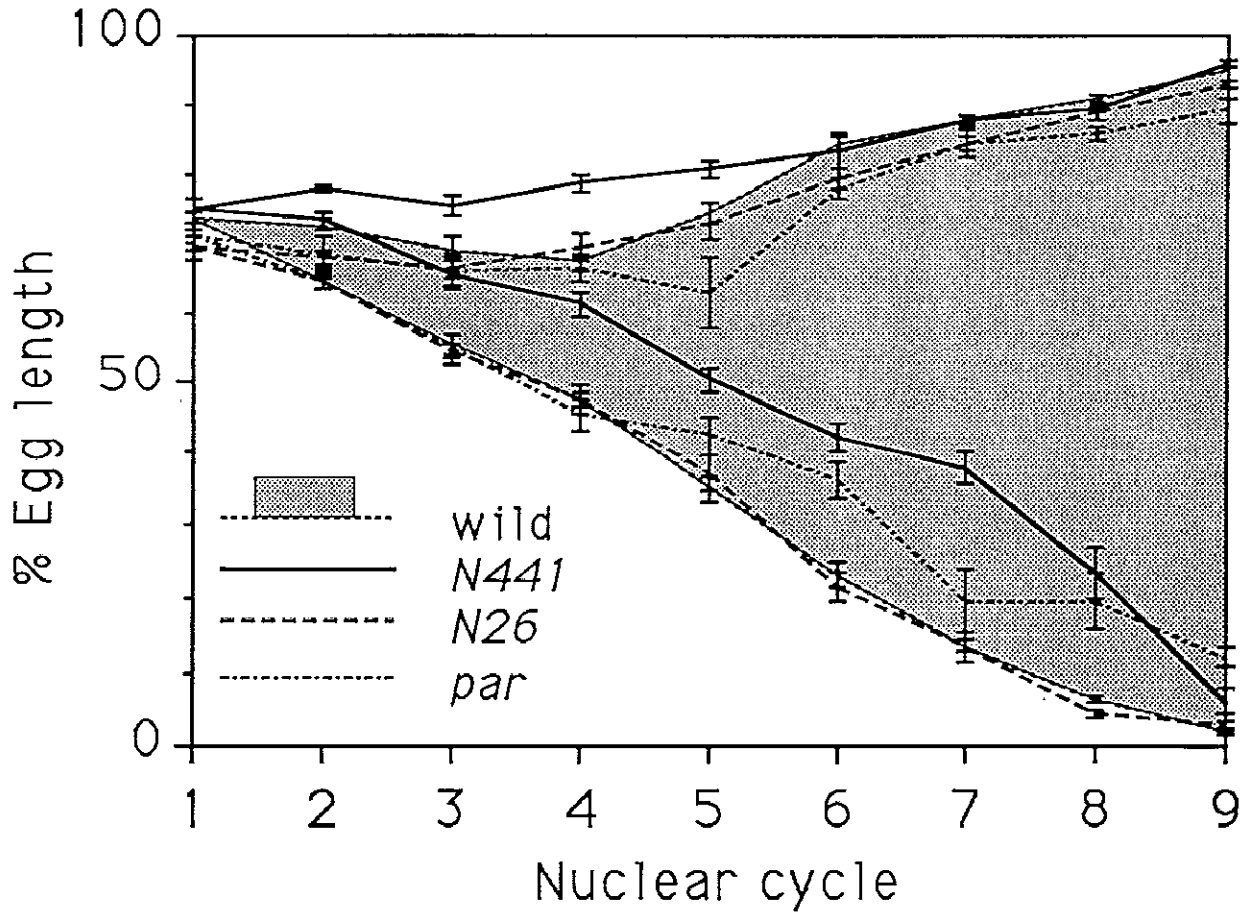
100
50
0
% Egg length
wild
N441
N26
par
1
2
3
4
5
6
7
8
9
Nuclear cycle

Fig. 6. Change in the range of nuclear distribution along the anteroposterior axis throughout the cleavage stages in the embryos from heterozygous mutant mothers raised at 25°C. The positions of the most anterior and the most posterior nuclei presented in Table 3 are visualized in this figure. Nuclear distribution is represented by the area limited by solid lines for N441/+, by broken lines for N26/+ and by dot-broken lines for par/+. The shaded area represents the range of nuclear distribution in the wild-type embryos from mothers raised at 25°C. 0% egg length indicates the posterior pole. Vertical bars represent standard errors.

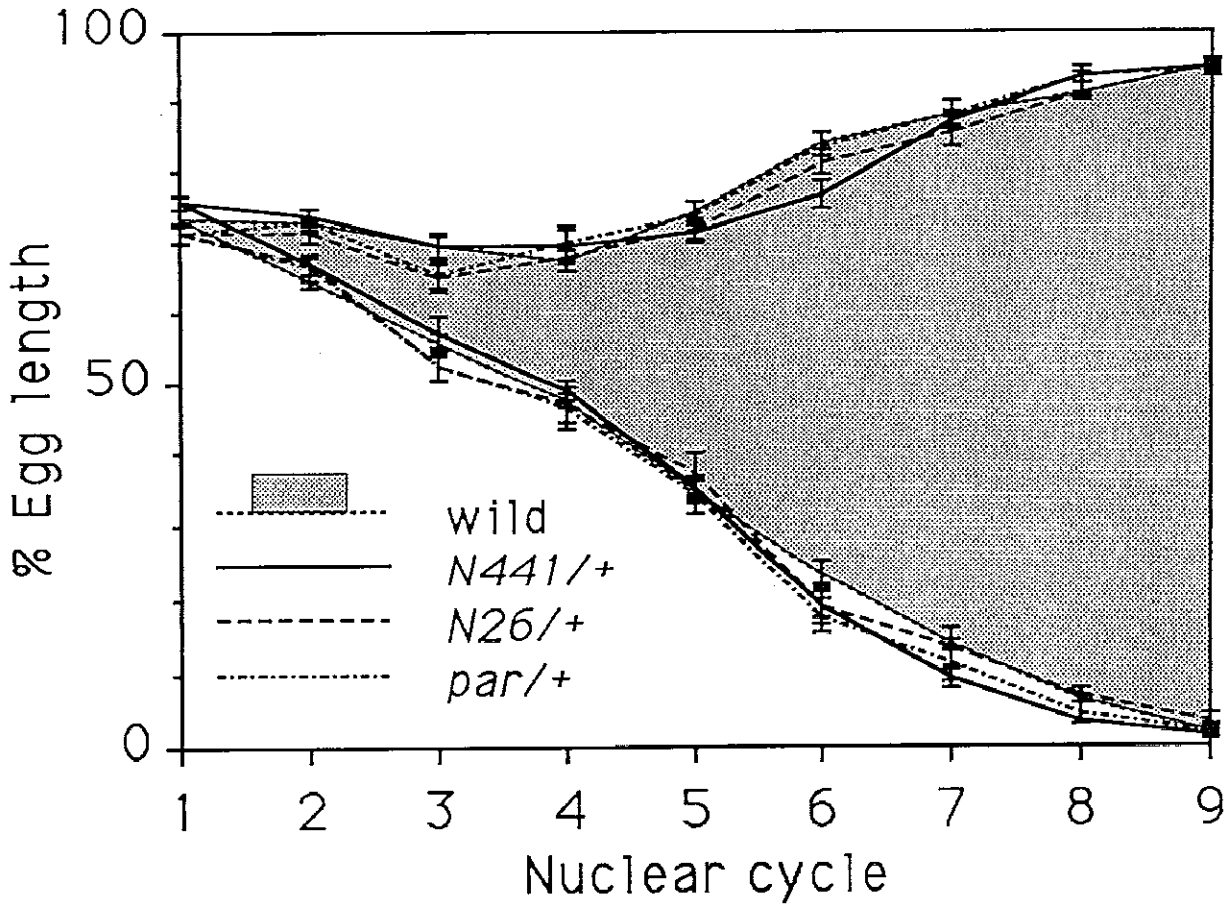
100
50
0
% Egg length
wild
N441/+
N26/+
par/+
1
2
3
4
5
6
7
8
9
Nuclear cycle

Fig. 7. Nuclear penetration of the cortex, and mitoses in the cortex, observed in live embryos with a time-lapse video. (A), a wild-type embryo. (B), a typical N441 embryo from a homozygous mother raised under a restrictive condition. Dotted areas show the range of nuclear distribution in the egg cortex along the anteroposterior axis. In darkly dotted areas, cortical nuclei were not able to be observed because they were in mitotic metaphase to telophase. The numbers on the darkly dotted areas show respective nuclear cycles, which was determined by observations of fixed and stained embryos. The abscissa shows the time after the first nuclear penetration of the cortex. 0% egg length indicates the posterior pole.

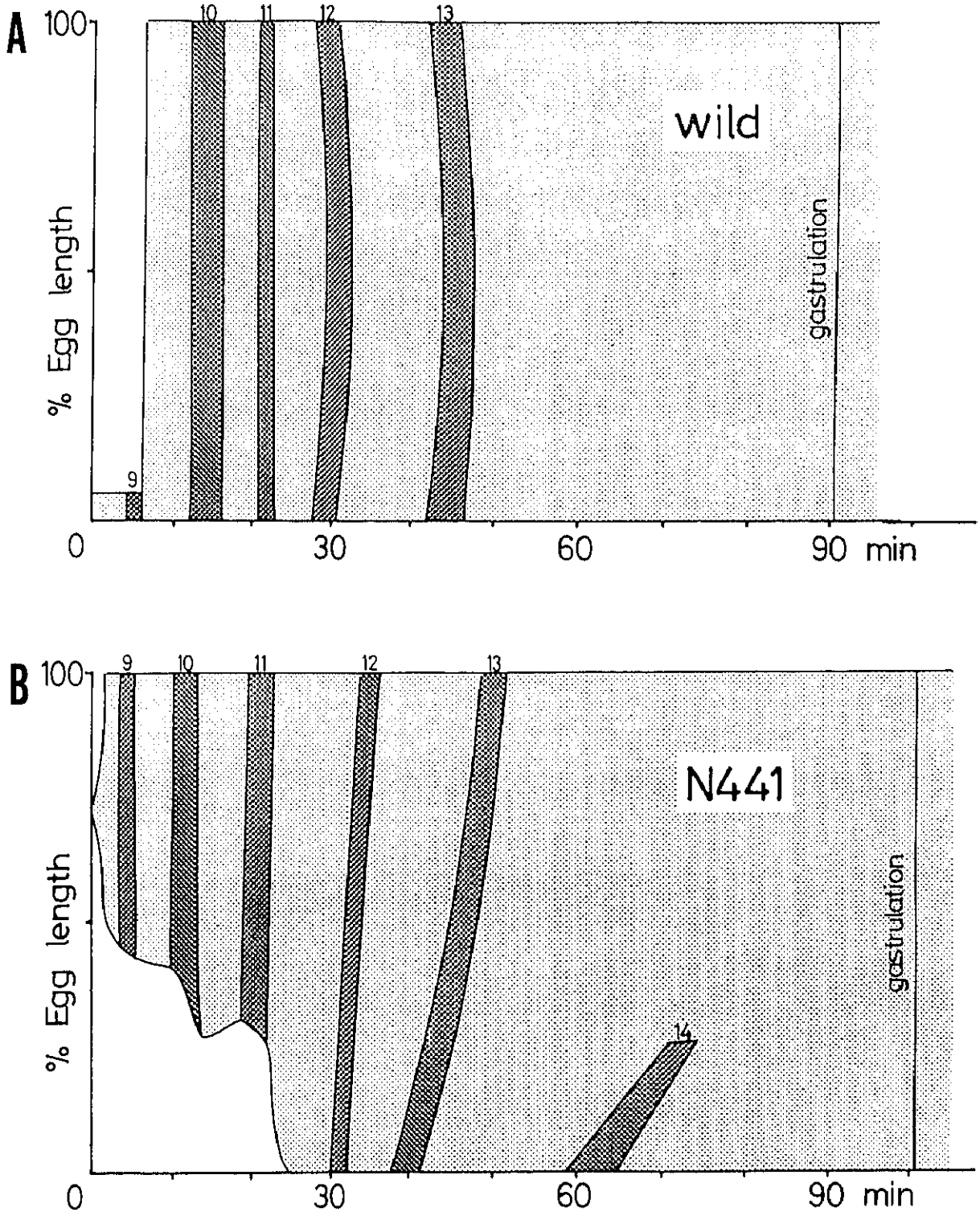
A
100
% Egg length
9
10
11
12
13
wild
gastrulation
0
30
60
90 min
B
100
% Egg length
9
10
11
12
13
14
N441
gastrulation
0
30
60
90 min

Fig. 8. Timing of nuclear penetration of the posterior pole cortex. Embryos were scored in each nuclear cycle when at least one nucleus had penetrated the posterior cortex in stained serial sections. Open circles represent wild-type embryos, filled circles represent N441 embryos from homozygous mothers raised under a permissive condition, and triangles represent N441 embryos from homozygous mothers raised under a restrictive condition.

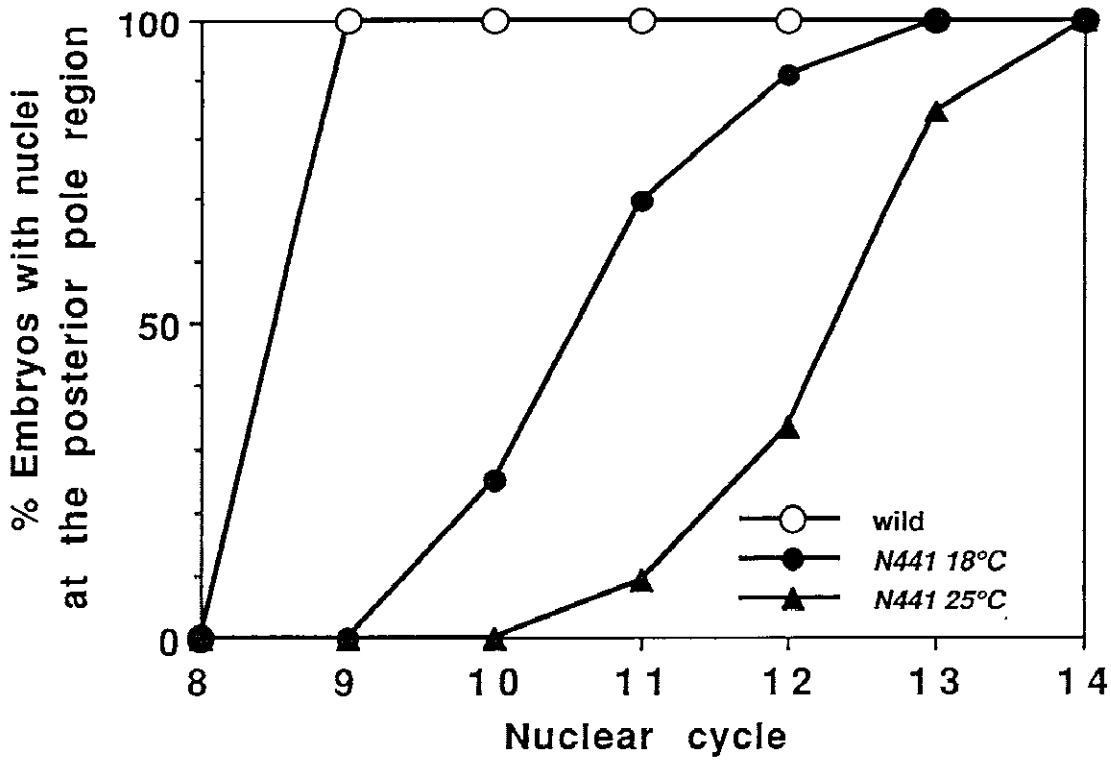
% Embryos with nuclei
at the posterior pole region
100
50
0
8
9
10
11
12
13
14
Nuclear cycle
wild
N441 18°C
N441 25°C

Fig. 9. Fine structure of posterior pole region in N441 embryos. (A), a cycle-9 to -10 embryo from a homozygous mother raised under a restrictive condition. (B), a cycle-11 embryo from a homozygous mother raised under a permissive condition. Plasma membrane is infolding from the surface of the embryo between cortical nuclei (not shown) in (B). A complex morphology at the tip of infolding plasma membrane is typical of the formation of blastodermal pole cells. Arrowheads indicate polar granules. Arrows indicate multivesicular bodies. Bar represents 1 μm.

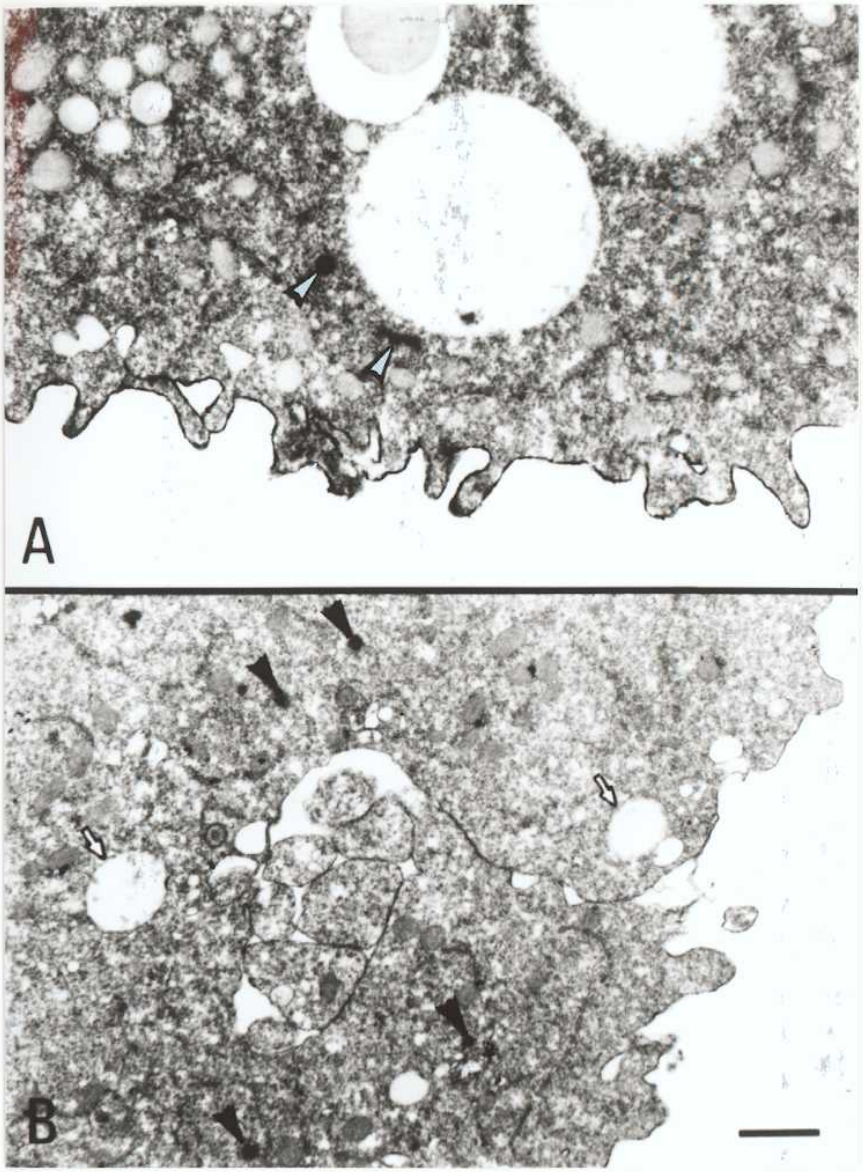
A
B

Fig. 10. Defects in segment pattern in N441 embryos. (A), a wild-type first instar larva. (B)-(D), N441 embryos from homozygous mothers raised under a restrictive temperature. In (B), the 4th and the 5th abdominal segments are fused, and so do the 6th and the 7th. In (C), complex cross-over fusions of abdominal segments are conspicuous. In (D), malformed mouth parts, deletions of segments in the thorax and the abdomen as well as paired fusion of some abdominal segments are recognizable. Bar represents 100 μm.

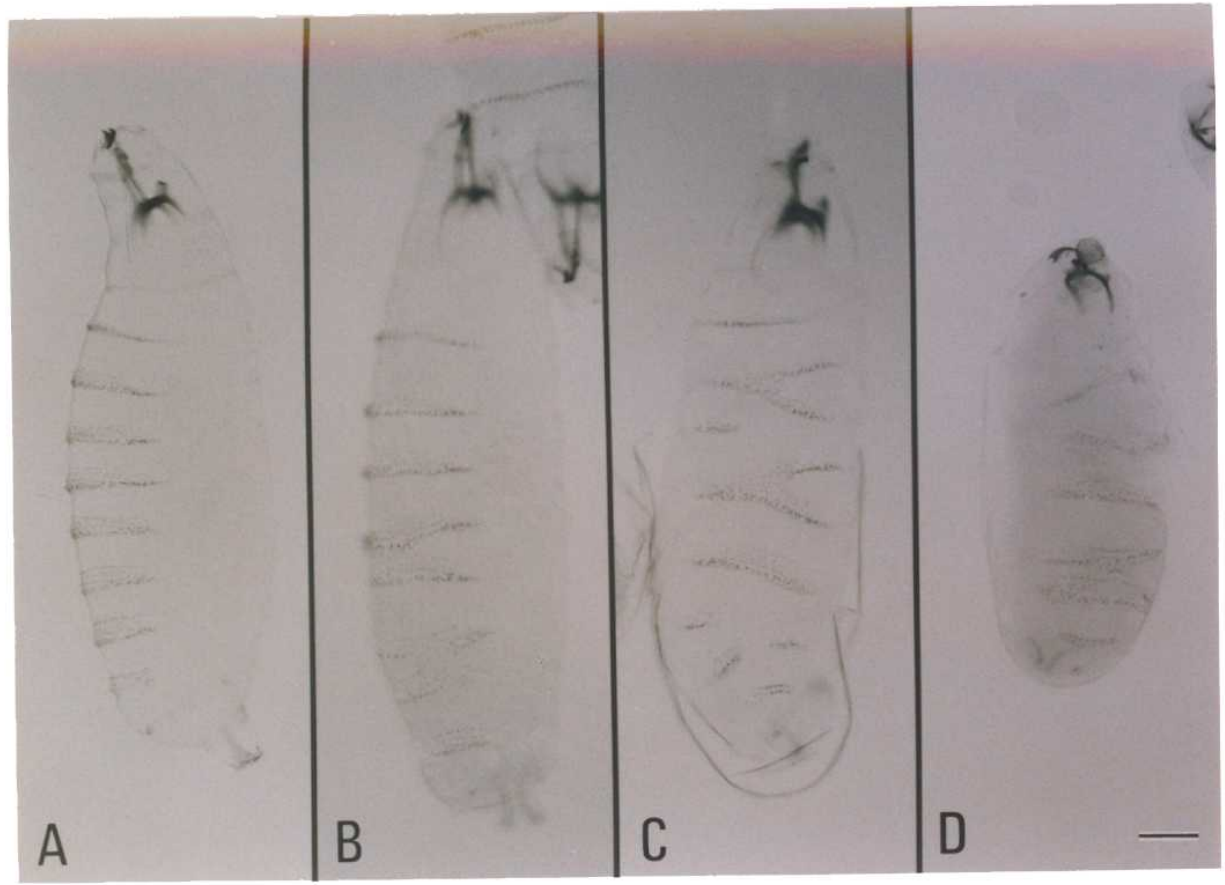
A
B
C
D

Fig. 11. Effects of cytoskeletal inhibitors on nuclear migration. (A), an untreated wild-type embryo at cycle 7; (B), a cycle-7 wild-type embryo treated with 1 µg/ml cytochalasin B for 5 min at cycle 2; (C), a cycle-7 wild-type embryo treated with 0.2 µg/ml colchicine for 5 min at cycle 2. Nuclei were stained with basic fuchsin (A, B), or with DAPI (C). Arrowheads in (B, C) indicate the most anterior and the most posterior nuclei in each embryo. Anterior poles are to the top. Bar represents 100 µm.

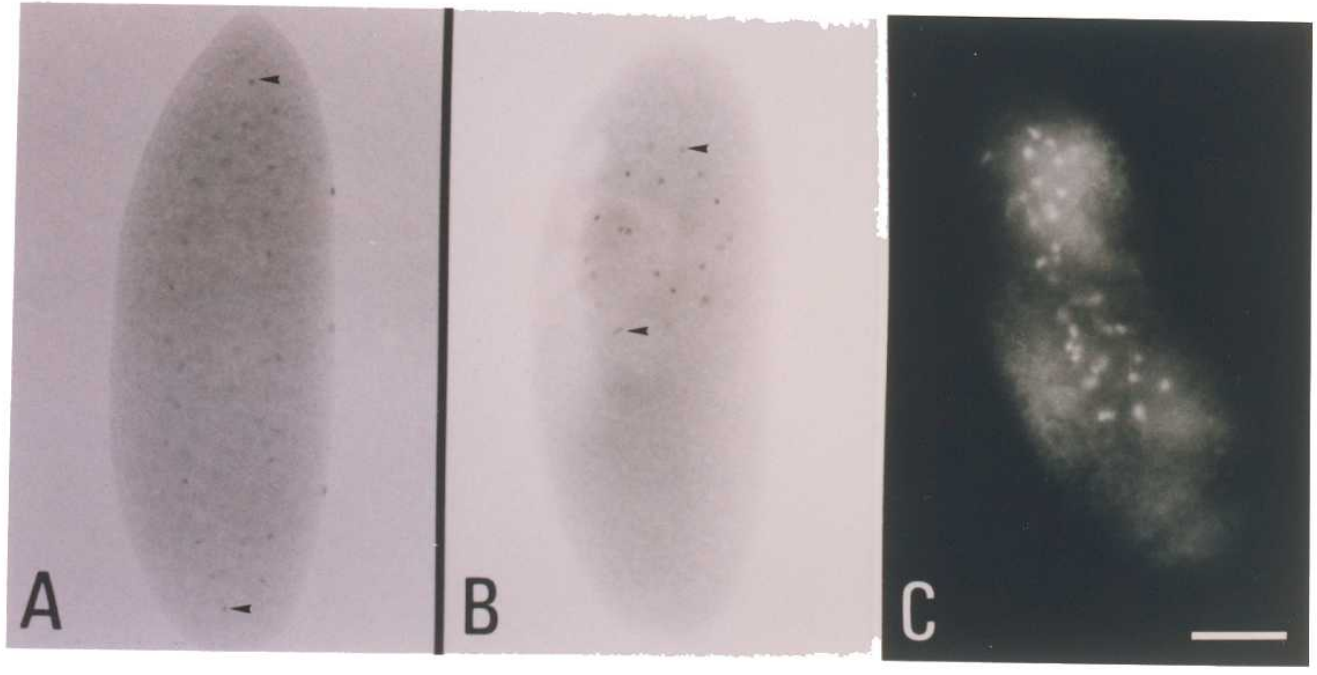
A
B
C

Fig. 12. Effects of colchicine, lumicolchicine and a mutation, RW630 on nuclear migration. Cycle-8 embryos are shown. Nuclei were stained with DAPI. (A), an untreated wild-type embryo; (B), a wild-type embryo treated with 0.2 µg/ml colchicine for 5 min at cycle 3; (C), an RW630 embryo; (D), a wild-type embryo treated with 10 µg/ml lumicolchicine for 5 min at cycle 3.

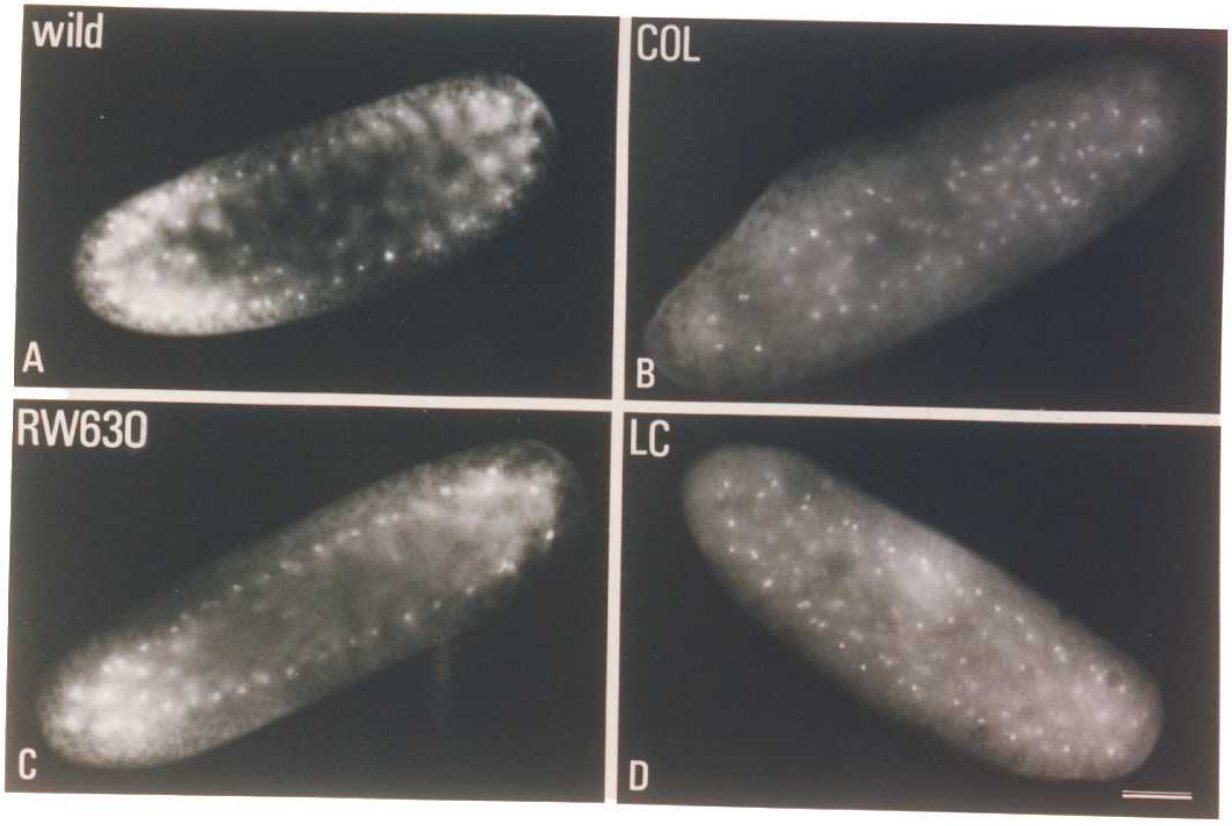
wild
A
COL
B
RW630
C
LC
D

Fig. 13. Nuclear migration toward the lateral egg cortex during late cleavage stages in wild-type (open circles) and RW630 (filled circles) embryos. The ordinate indicates the range of nuclear distribution in percentage of the egg width in the middle region of the anteroposterior axis of embryos. Vertical bars represent standard errors.

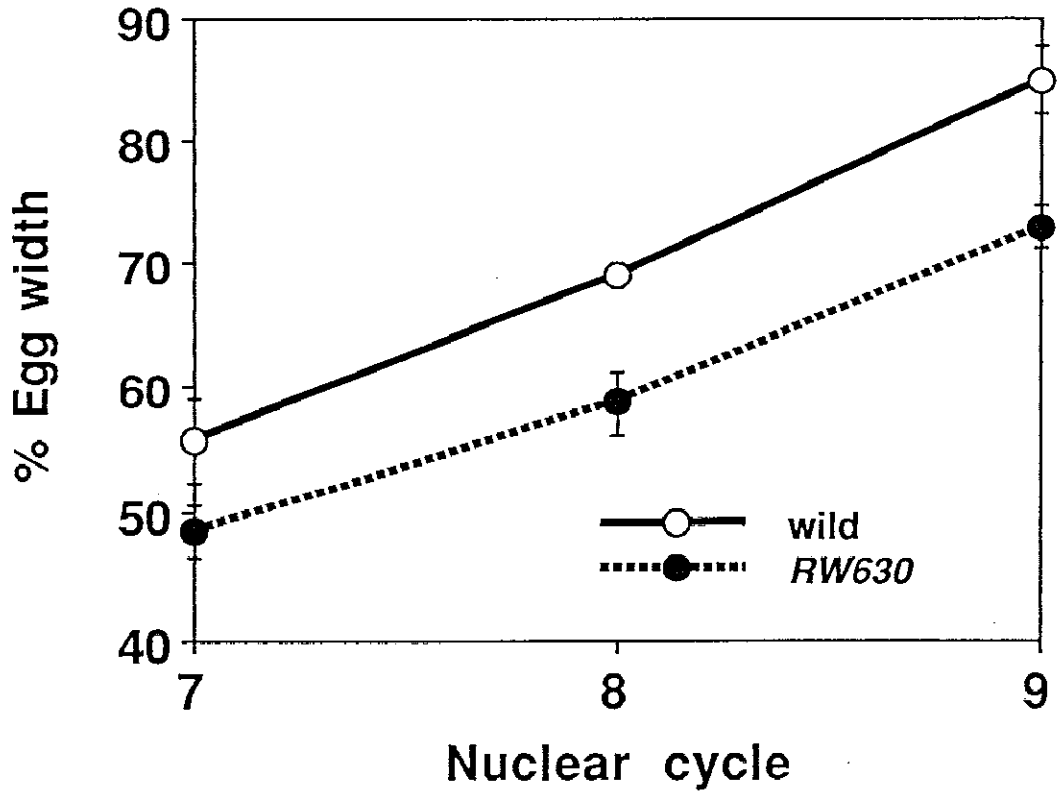
90
80
70
60
50
40
% Egg width
7
8
9
Nuclear cycle
wild
RW630

Fig. 14. Effects of cytoskeletal inhibitos and a mutation, RW630 on the cortical nuclear distribution at syncytial blastoderm stages. Nuclei were stained with DAPI. (A), a cycle-11 wild-type embryo; (B), a cycle-11 RW630 embryo; (C), a cycle-10 wild-type embryo treated with 0.2 µg/ml colchicine for 5 min at cycle 8; (D), a wild-type syncytial blastoderm embryo treated with 1 µg/ml cytochalasin B for 5 min at cycle 8. Bar represents 50 µm.

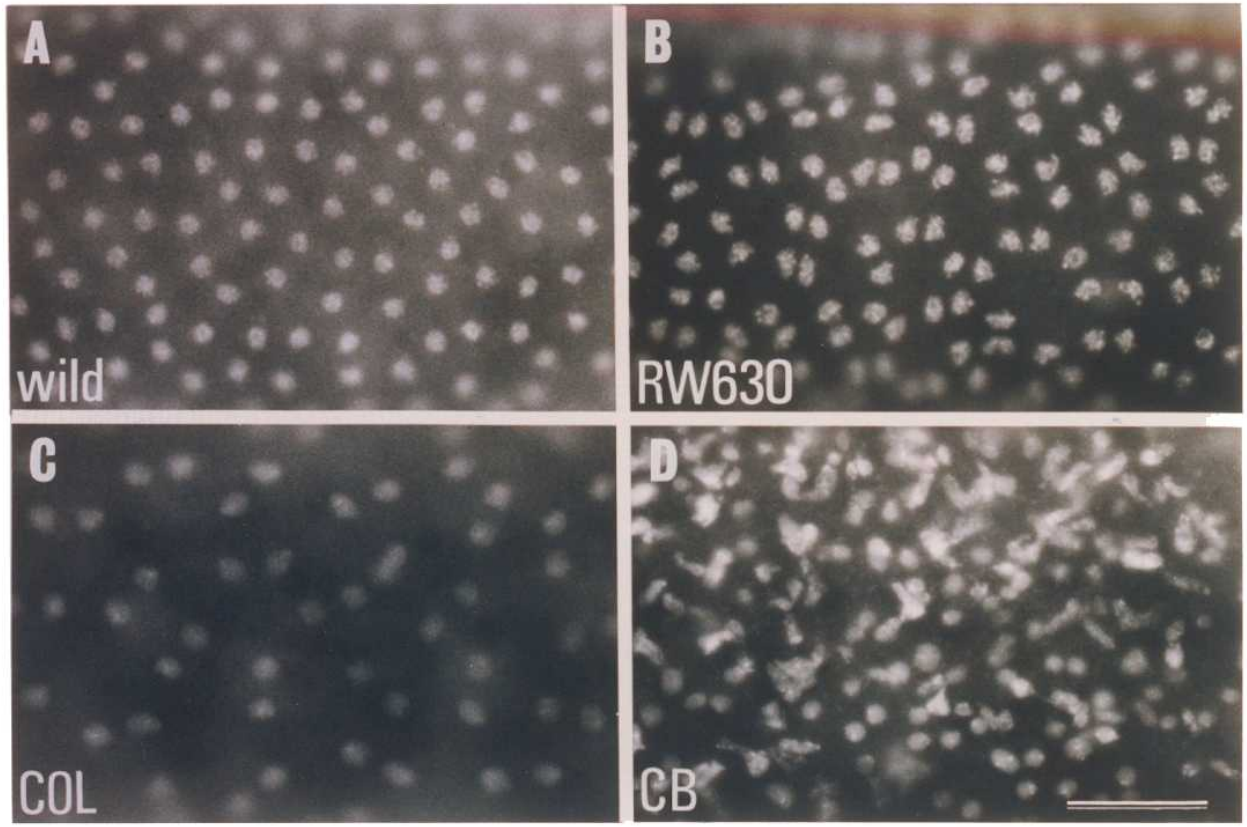
A
wild
B
RW630
C
COL
D
CB

Fig. 15. Measurement of three-dimensional nuclear position at cycle 1 and 2. (A), a cycle-1 embryo; (B), a cycle-2 embryo; (C), posterior view of (B). ap: anterior pole, pp: posterior pole, pbn: polar body nucleus, an: anterior nucleus, pn: posterior nucleus, gs: glass slide. d_x, d_y and d_z represent lateral, anteroposterior and vertical coordinate axis elements of the actual distance between two nuclei, respectively. d_o represents the distance between two nuclei measured on the lateral perspective. p and q represent vertical and lateral coordinate axis elements of the distance between the center of the polar body nuclus and the midpoint of two nuclei, respectively.

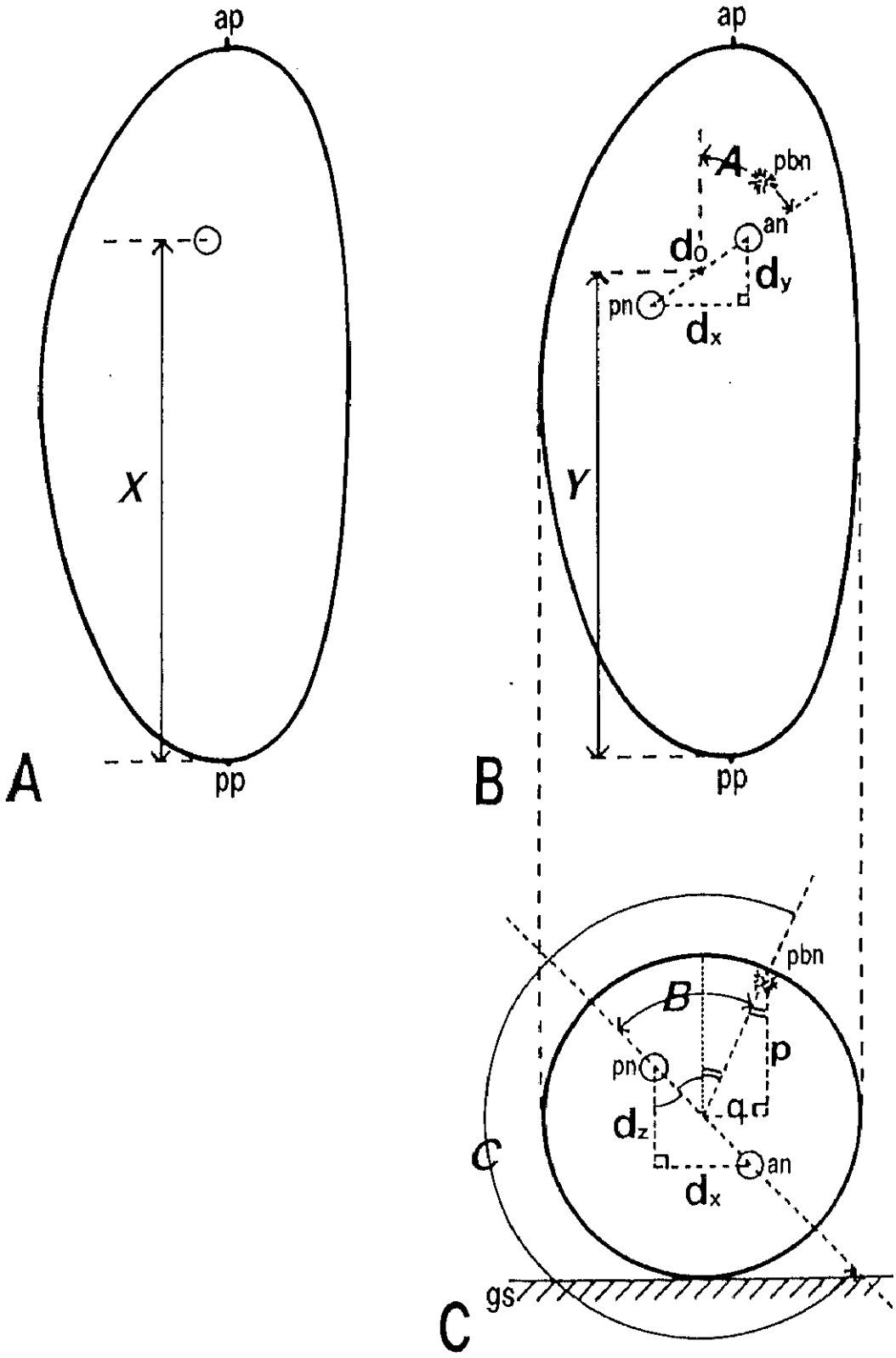
ap
X
pp
A
ap
A
pbn
an
d_o
d_y
pn
d_x
Y
pp
B
pbn
B
p
pn
q
d_z
an
d_x
C
gs
C

Fig. 16. Specificity of the staining of F-actin with rhodaminyl phalloidin. (A), a wild-type embryo at cycle 5 which was double-stained with DAPI and rhodaminyl phalloidin, and observed under U.V. light for exciting DAPI; (B), the same embryo as in (A) observed under green light for exciting rhodaminyl phalloidin. (C), a wild-type embryo stained with only DAPI and observed under green exciting light as in (B), showing no auto-fluorescence. (D), a wild-type embryo pretreated with 1 mg/ml phalloidin for 15 min, stained with DAPI and rhodaminyl phalloidin, and observed under green exciting light, showing no non-specific binding of rhodaminyl phalloidin. Bar represents 50 μm.

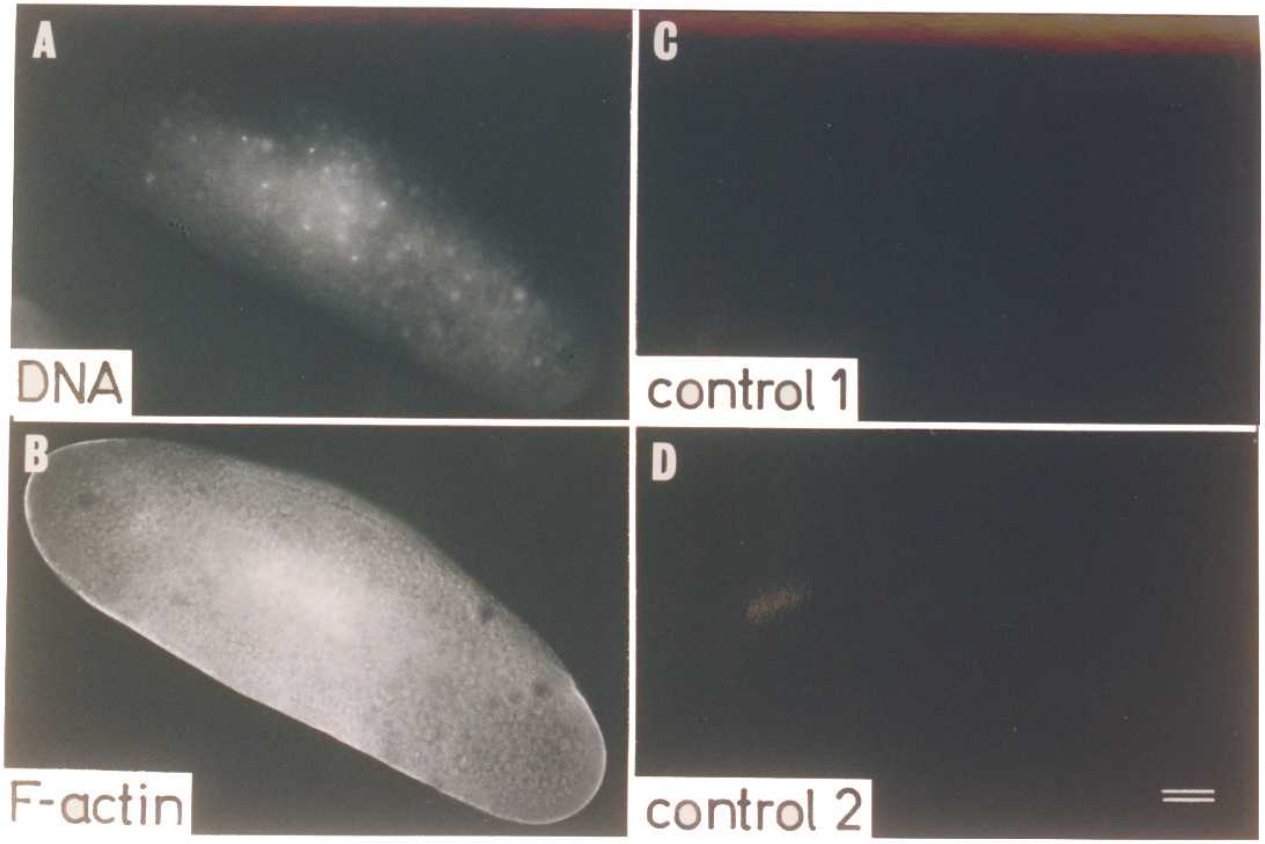
A
DNA
C
control 1
B
F-actin
D
control 2

Fig. 17. The distribution of F-actin in wild-type embryos. Embryos were stained with rhodaminyl phalloidin (A, C and E), or with DAPI (B and D). (A) and (B), the same cycle-2 embryo; (C) and (D), the same cycle-3 embryo; (E), the anterior region of a cycle-3 embryo. Whole mount embryos are shown. (E), confocal images. Anterior poles are to the top in (A)-(D) and to the top-left corner in (E). Arrowheads in (A), (C) and (E) indicate the central domain of F-actin. A 30 μm-thick F-actin-enriched layer is indicated between arrows in (E). In the wild-type strain used for the present study, DAPI binds not only to nuclei but also to the granular structures localized around the poles of mitotic spindles (arrows in D) and in the posterior polar plasm. Bars represent 50 μm.

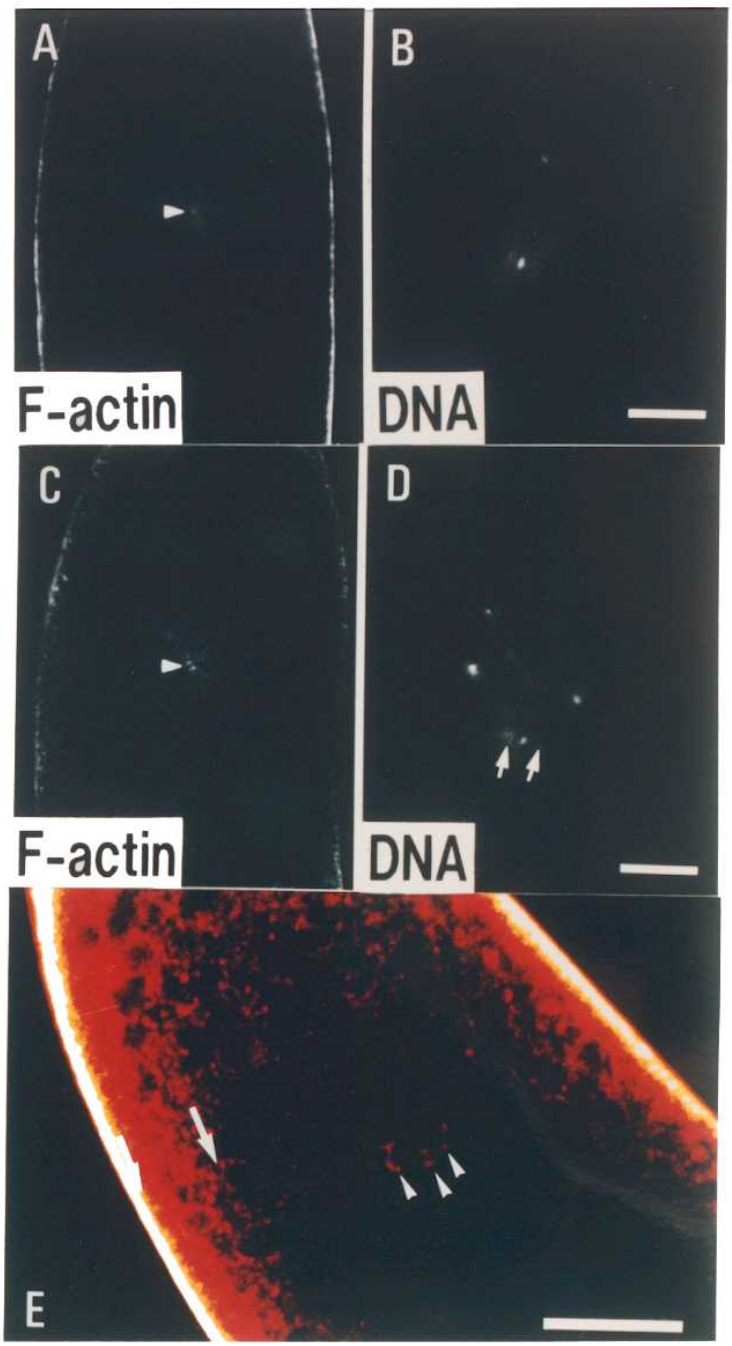
A
B
F-actin
DNA
C
D
F-actin
DNA
E

Fig. 18. The distribution of F-actin in wild-type embryos. Embryos were stained with rhodaminyl phalloidin (A and C), or with DAPI (B and D). (A) and (B), the same cycle-2 embryo; (C) and (D), the same cycle-3 embryo. Whole mount embryos are shown. Anterior poles are to the top. Arrowheads in (A) indicate the central domain of F-actin; in (C) indicate energid domains of F-actin. A bright spot in (A) is an artifact, the influence of which is limited topically. Arrows in (D) indicate the DAPI-stained granular structures localized around the poles of mitotic spindles. Bars represent 50 μm.

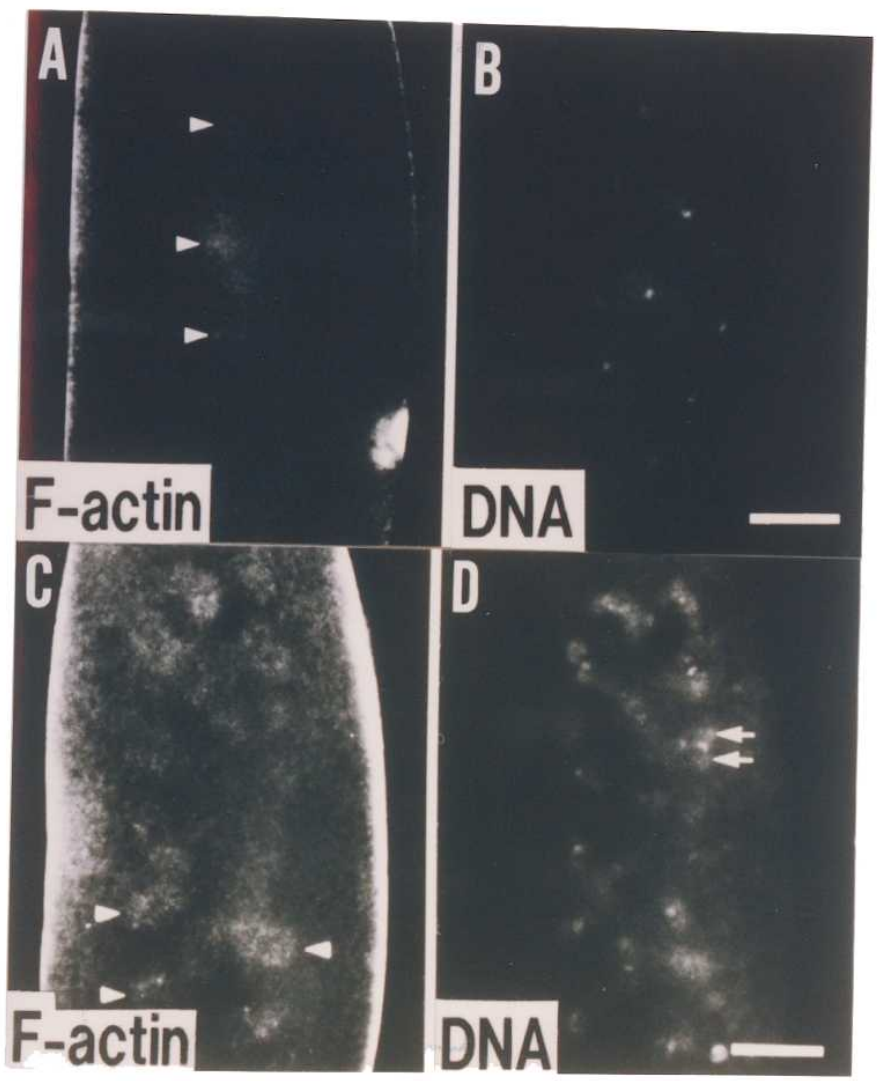
A
B
F-actin
DNA
C
D
F-actin
DNA

Fig. 19. The distribution of F-actin in a frozen section of a wild-type embryo at cycle 6. (A) and (B) show the same section of a double-stained embryo. (A), rhodaminyl phalloidin staining; (B), DAPI staining. The anterior pole is to the left. Arrowheads in (B) indicate the DAPI-stained granular structures as shown in Figs. 17 and 18. Bar represents 50 μm.

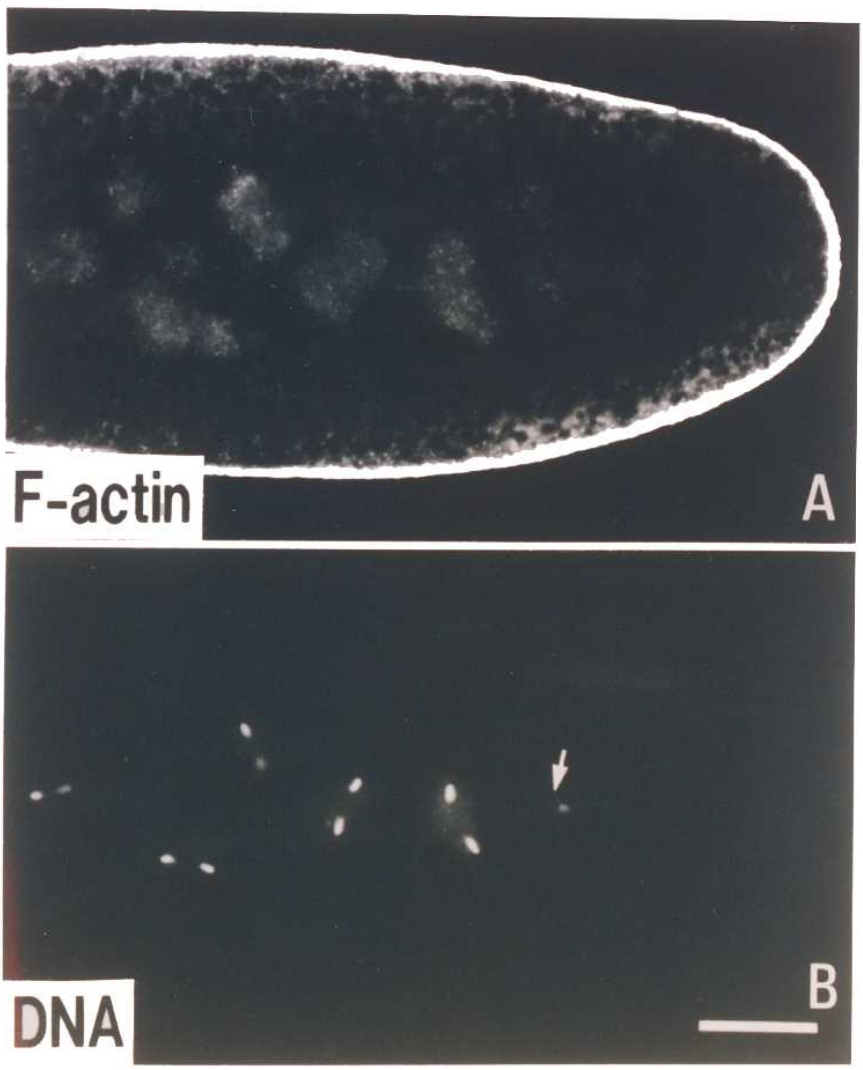
F-actin
A
DNA
B

Fig. 20. The distribution of F-actin in the posterior region of a wild-type embryo at cycle 11. A confocal image of a whole mount embryo stained with rhodaminyl phalloidin is shown. The anterior pole is to the top-left corner. Arrowheads indicate a deeper layer of F-actin surrounding the central yolk mass. Bar represents 50 μm.

TOP

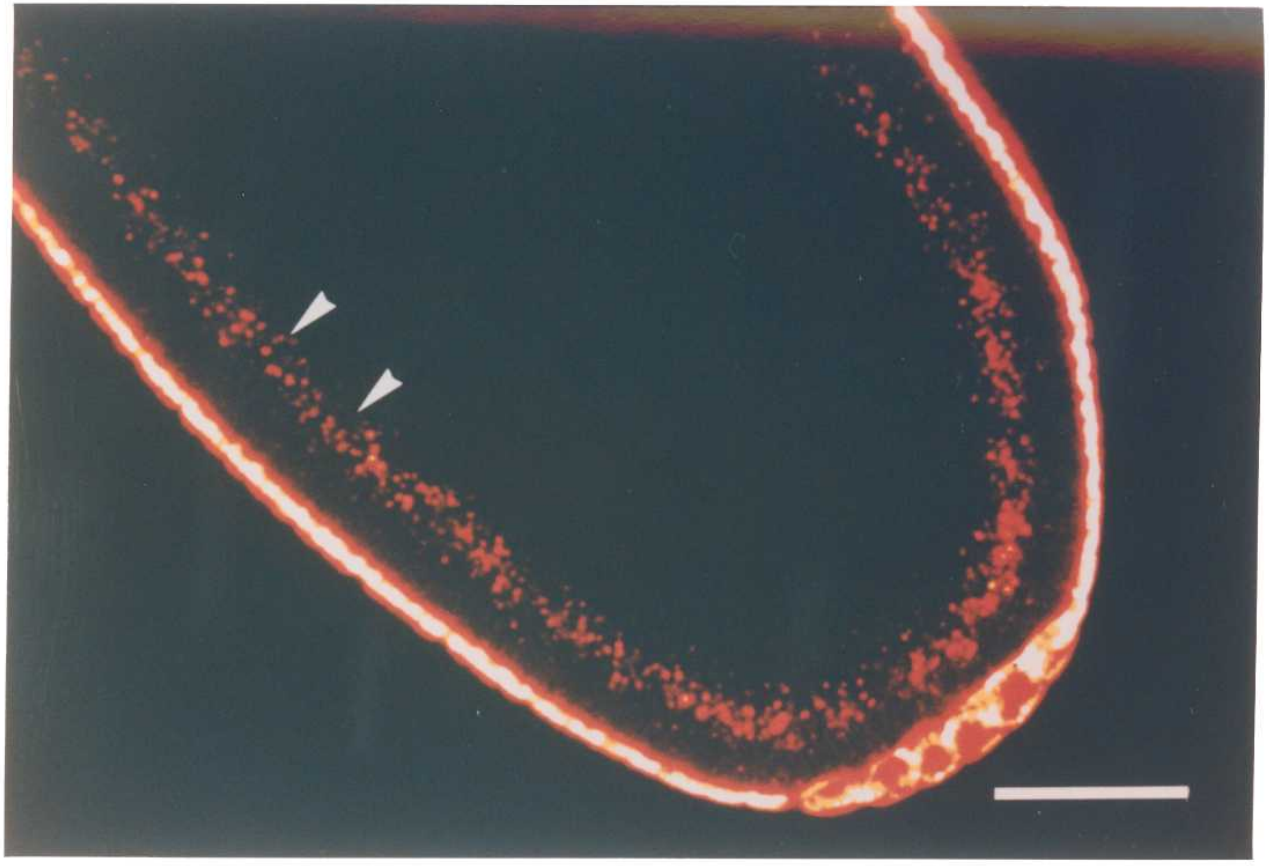

Fig. 21. Cortical F-actin in cleavage embryos. Embryos were stained with rhodaminyl phalloidin. Wild-type (A), N441 (B), N26 (C) and par (D) embryos are shown. Focus is on the surface of whole mount embryos. Anterior poles are to the left. Bar represents 100 μm.

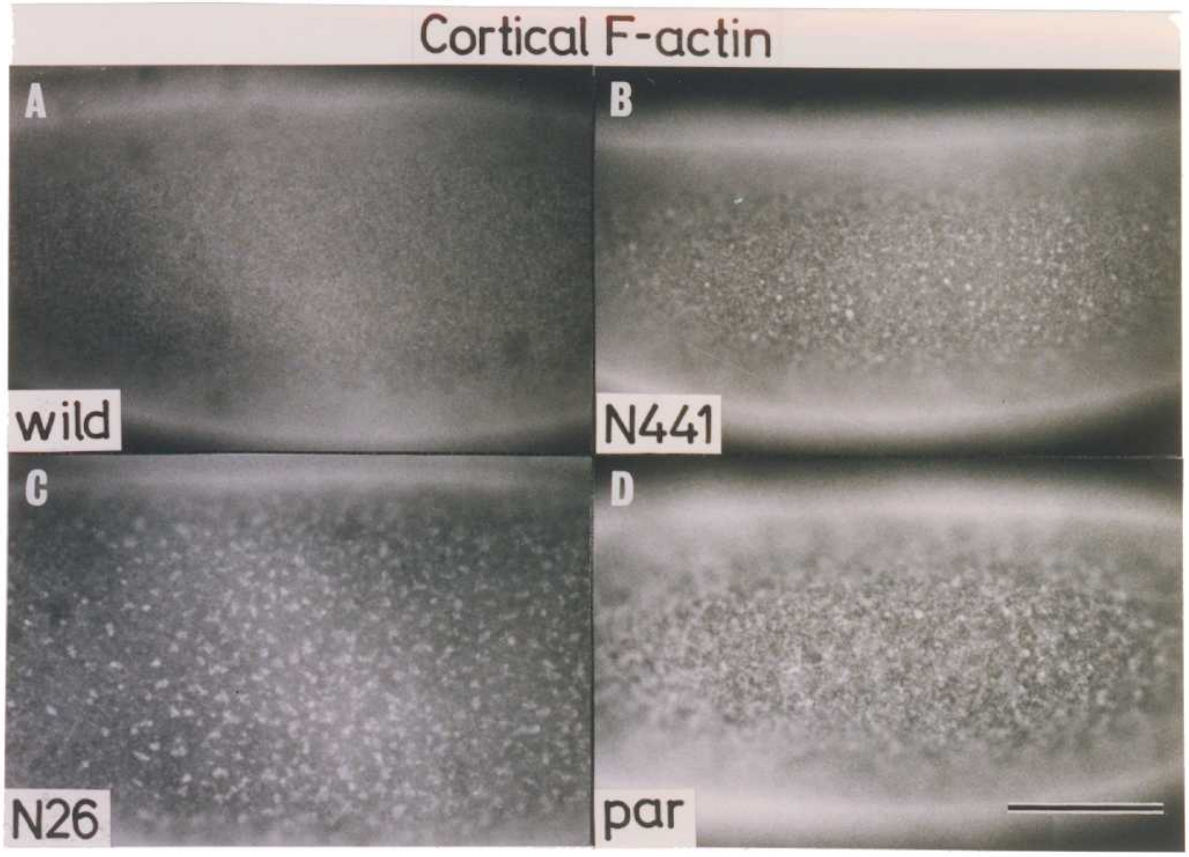
Cortical F-actin
A
wild
B
N441
C
N26
D
par

Fig. 22. Cortical F-actin in cleavage embryos. Embryos were stained with rhodaminyl phalloidin. Wild-type (A), N441 (B), N26 (C) and par (D and E) embryos are shown. Focus is on the margin of whole mount embryos in (A)-(D), and just beneath the surface of the embryo in (E). Arrowheads indicate mutant-type cortical F-actin aggregates. (E), a confocal image showing small open spherical shape of several cortical F-actin aggregates. Bar represents 100 μm in (A)-(D), 50 μm in (E).

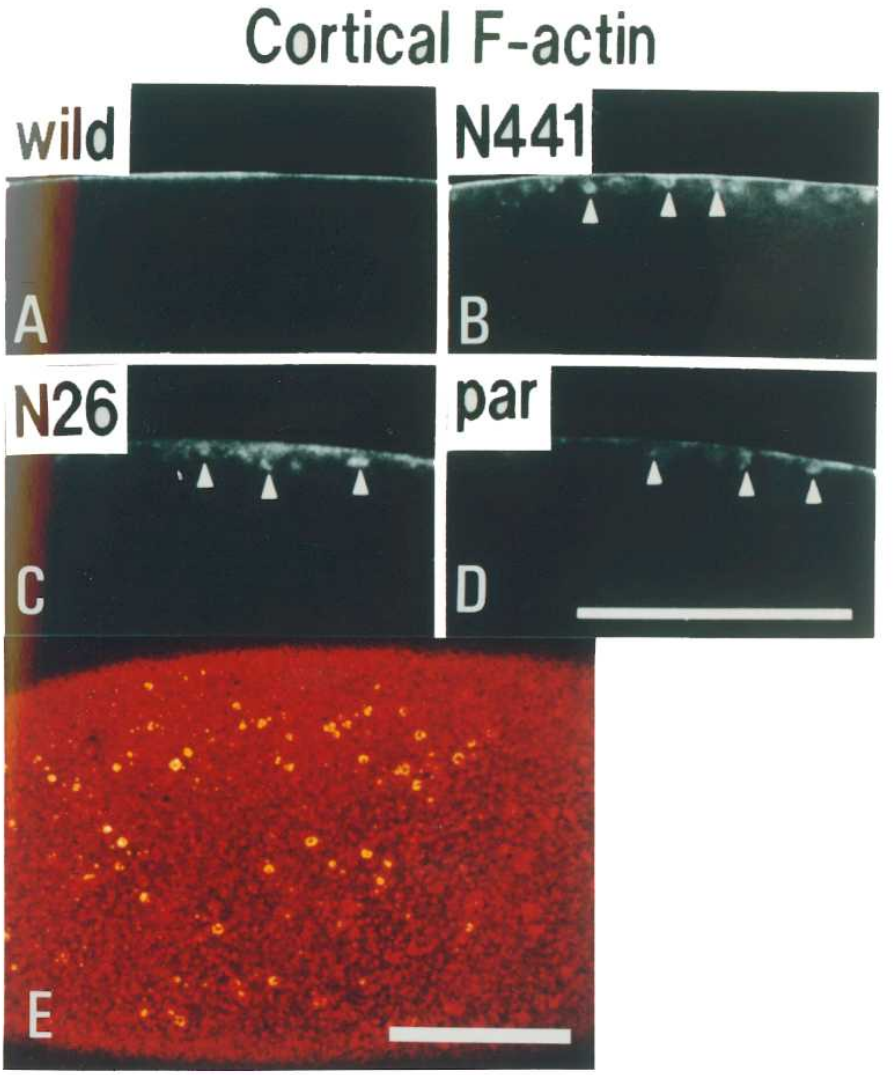
Cortical F-actin
wild
N441
A
B
N26
par
C
D
E

Fig. 23. Normal cortical F-actin organization restored to mutant embryos after nuclear arrival in the cortex. Rhodaminyl phalloidin-stained N26 embryos at cycle 9 (A) and at a late syncytial blastoderm stage (C) showing cortical F-actin. Nuclei of the same embryos shown in (A) and (C) are visualized by DAPI staining in (B) and (D), respectively. Focus is slightly deeper in (B) than in (A). Anterior poles are to the top-right corner. Bar represents 100 μm.

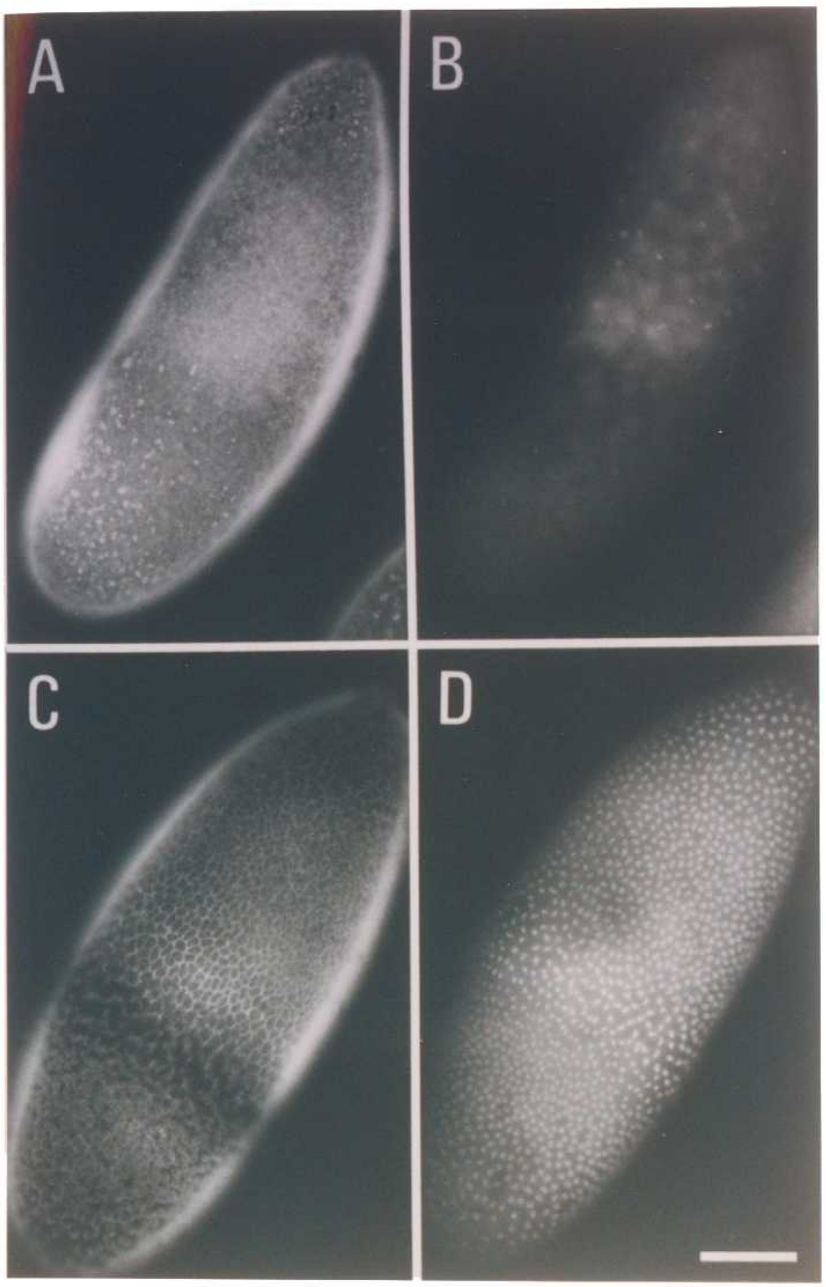
A
B
C
D

Fig. 24. Normal cortical F-actin organization restored to mutant embryos at a late syncytial blastoderm stage. Rhodaminyl phalloidin-stained N441 (B) and par (D) embryos showing cortical F-actin. Nuclei of the same embryos shown in (B) and (D) are visualized by DAPI staining in (A) and (C), respectively. Anterior poles are to the top-left corner in (A) and (B), to the bottom-left corner in (C) and (D). Bar represents 50 μm.

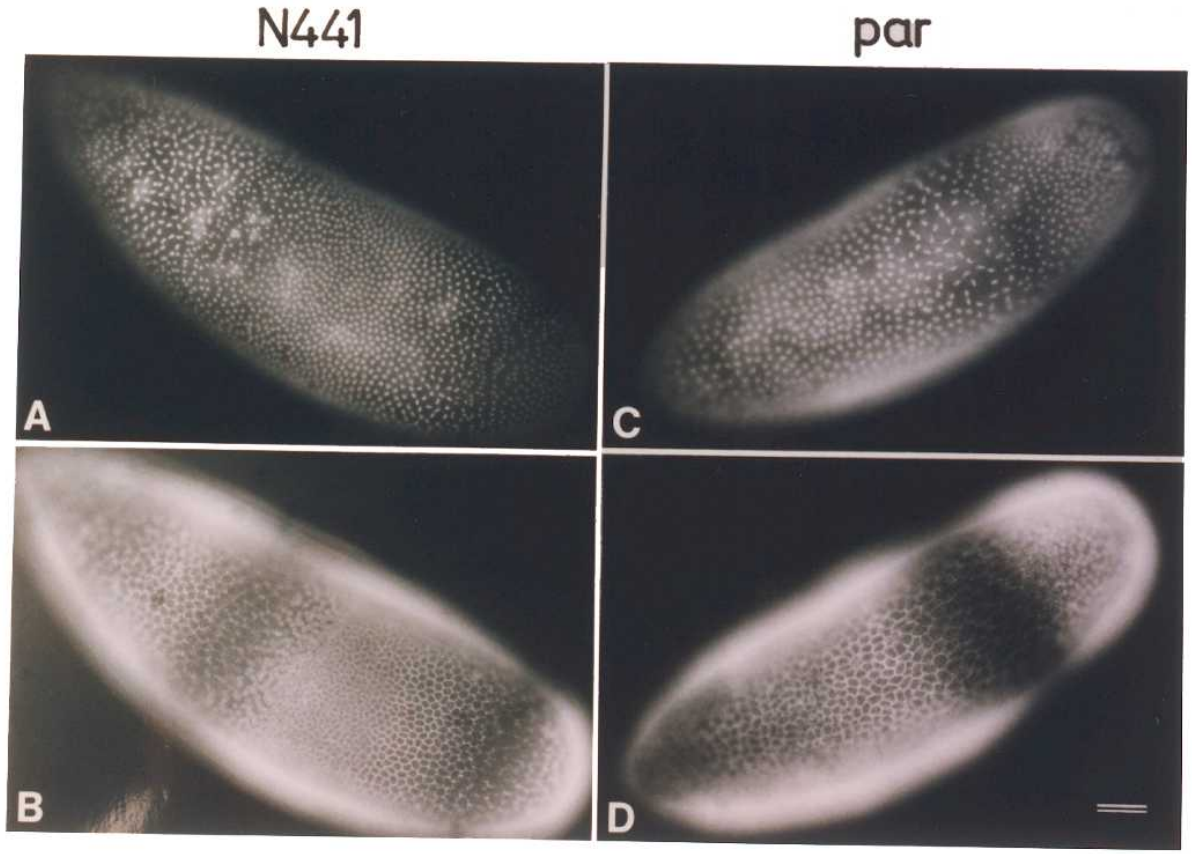
N441
par
A
C
B
D

Fig. 25. F-actin distribution in mutant embryos. Embryos were stained with rhodaminyl phalloidin in (A), (C) and (E); with DAPI in (B) and (F). (D), an interference contrast image of (C) showing energids (black arrowheads). (A), an N441 embryo at cycle 6; (C), an N26 embryos at cycle 6; (E), a par embryo at cycle 7. (A and B), (C and D), and (E and F) are the combinations of the same double-stained embryos photographed with different excitation light, respectively. (A), (B), (E) and (F), anterior part of whole mount embryos; (C) and (D), the same frozen section of the anterior part of the embryo observed with different optics. The central domain of F-actin is shown between white arrowheads in (A), (C) and (E). Anterior poles are to the top. Bars represent 50 μm.

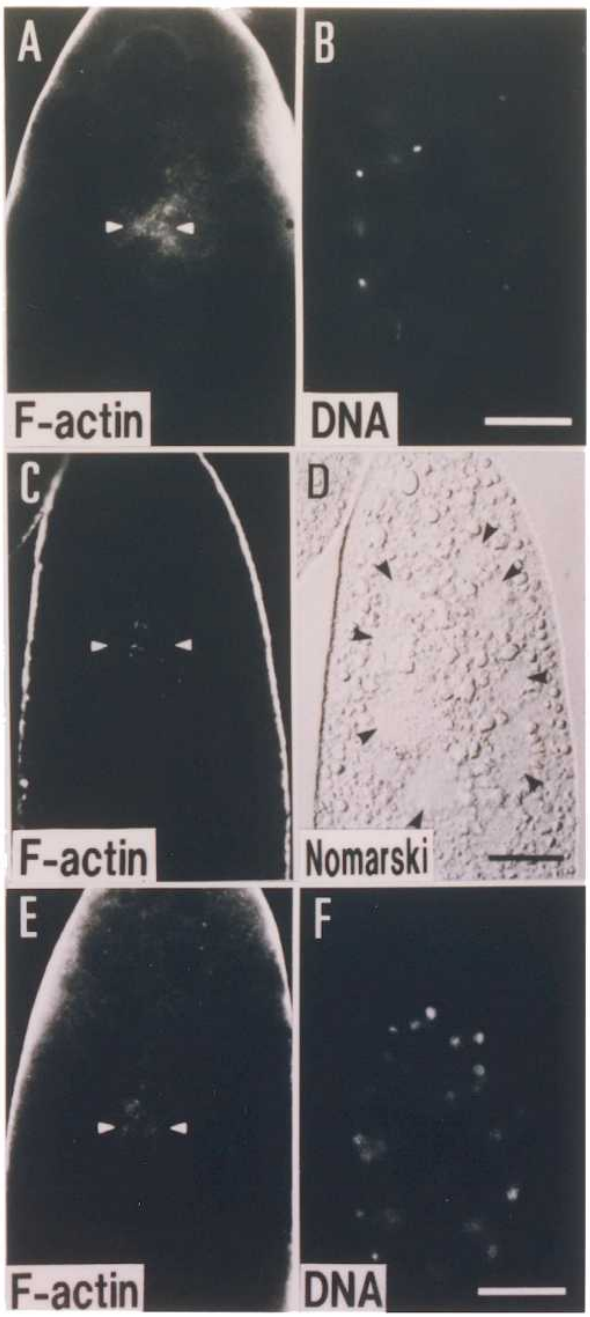
A
B
F-actin
DNA
C
D
F-actin
Nomarski
E
F
F-actin
DNA

Fig. 26. Confocal images of the anterior part of whole mount embryos stained with rhodaminyl phalloidin. (A), an N441 embryo at cycle 6; (B), an N26 embryo at cycle 8; (C), a par embryo at cycle 7. The central domains of F-actin are shown between arrowheads. Anterior poles are to the top in (A), to the top-left corner in (B) and (C). Bar represents 50 μm.

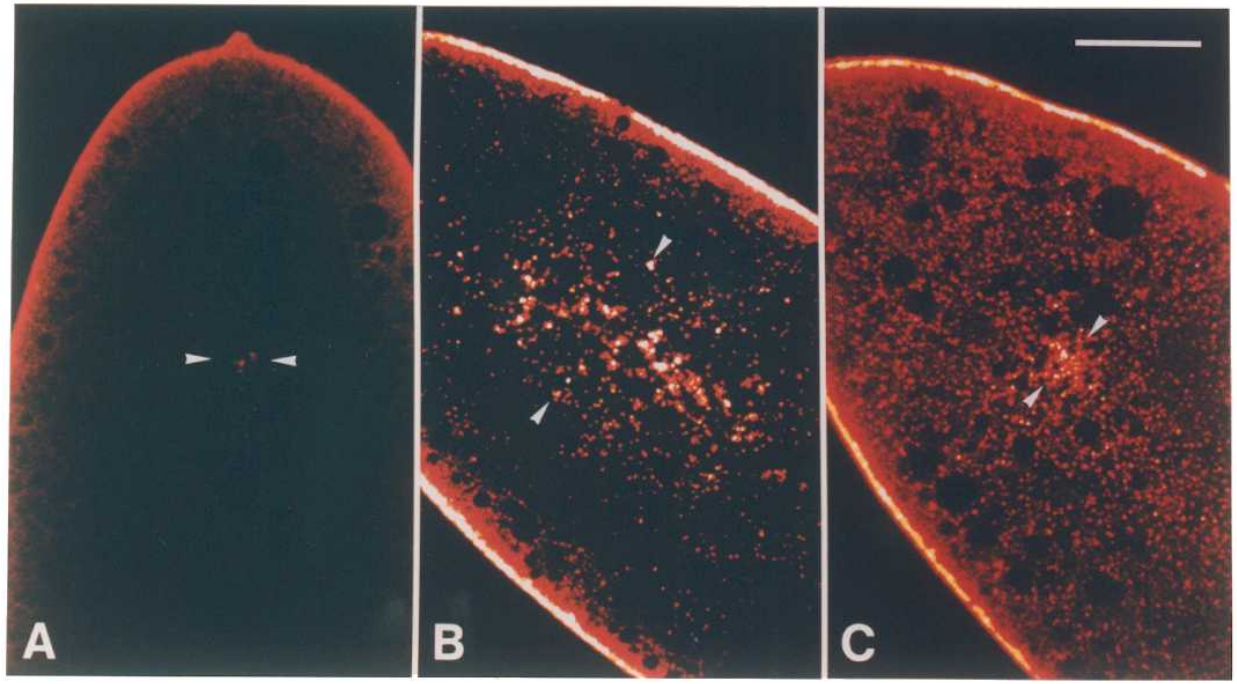
A
B
C

Fig. 27. A confocal image of the anterior part of a whole mount N26 embryo at cycle 9 stained with rhodaminyl phalloidin. Transition of F-actin distribution from the central domain (between arrowheads) to the energid domain (arrows) is probably in progress in this embryo. Anterior pole is to the left. Bar represents 50 μm.

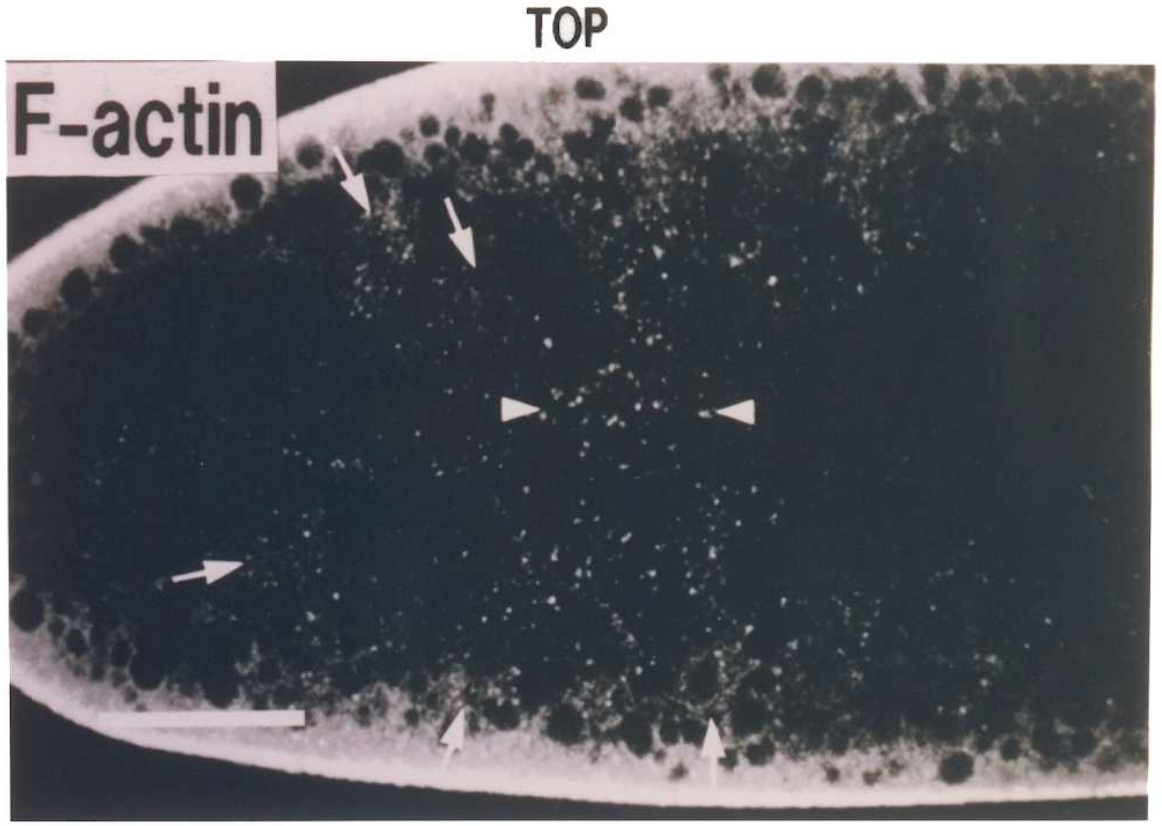
TOP
F-actin

Fig. 28. Schematic representation of the developmental changes in the distribution of nuclei and F-actin in wild-type (A-C) and mutant (D-F) embryos. Cycle-3 (A and D), cycle-5 (B and E) and cycle-7 (C and F) embryos are shown. Filled circles represent nuclei; shaded areas represent the regions where F-actin is detectable and crosses represent mutant-type F-actin aggregates in the cortex.

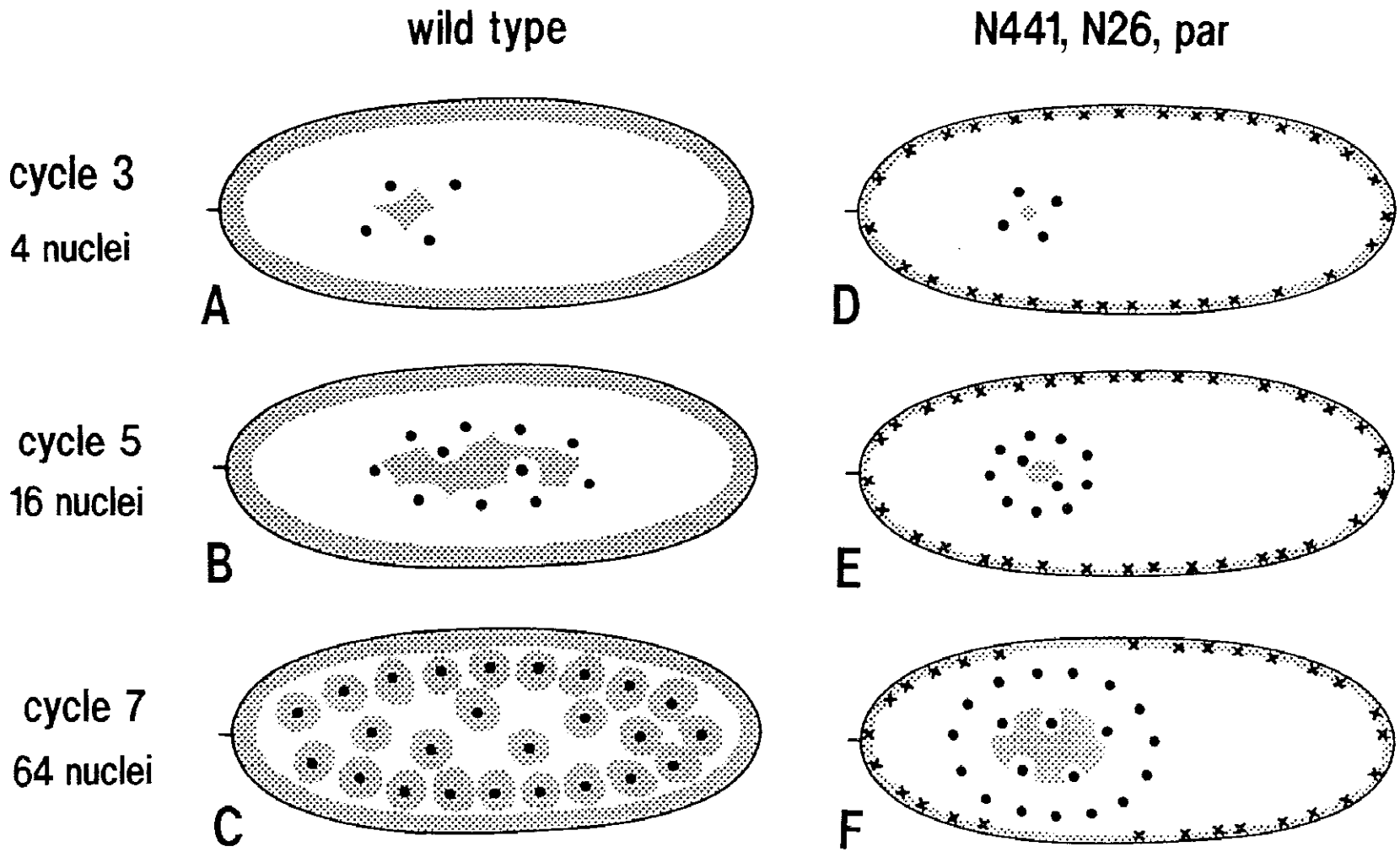
wild type
N441, N26, par
cycle 3
4 nuclei
A
D
cycle 5
16 nuclei
B
E
cycle 7
64 nuclei
C
F

Fig. 29. Fragmented cortical F-actin layer of wild-type embryos treated with 1 µg/ml cytochalasin B for 5 min at various stages. (A), a cycle-7 embryo treated at cycle 2; (B), a syncytial blastoderm embryo treated at cycle 8. (C), the same field shown in (B), but nuclei are visualized by DAPI staining. Focus is on the surface of whole mount embryos. Bar represents 50 µm.

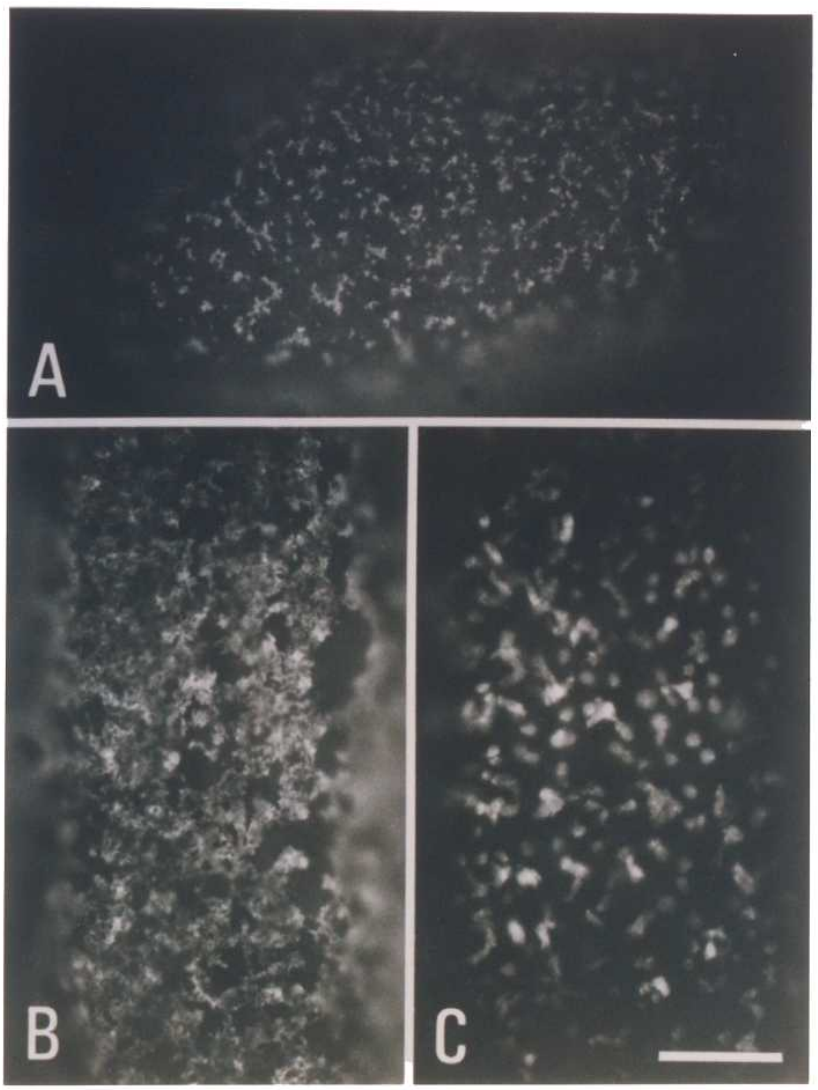
A
B
C

Fig. 30. Cortical F-actin in early syncytial blastoderm embryos. Wild-type (B), aur (D) and elD (F) embryos stained with rhodaminyl phalloidin are shown. (A), (C) and (E) are the same field shown in (B), (D) and (F), respectively, but nuclei were visualized with DAPI staining. Bar represents 50 μm.

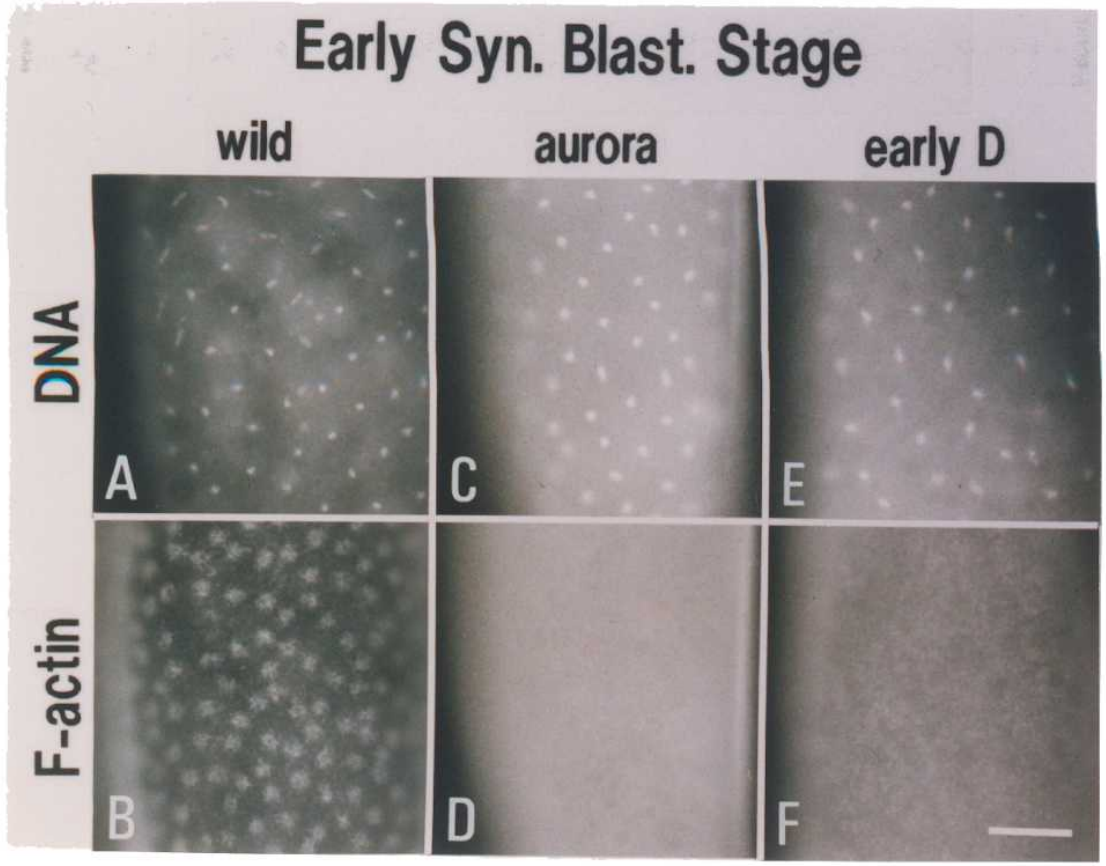
Early Syn. Blast. Stage
wild
aurora
early D
DNA
F-actin
A
B
C
D
E
F

Fig. 31. Cortical F-actin in late syncytial blastoderm embryos. Wild-type (B), aur (D), elD (F) embryos stained with rhodaminyl phalloidin are shown. (H), a wild-type embryo treated with 1 µg/ml cytochalasin B for 5 min at cycle 8. (A), (C), (E) and (G) are the same field shown in (B), (D), (F) and (H), respectively, but nuclei were visualized with DAPI staining. Bar represents 50 µm.

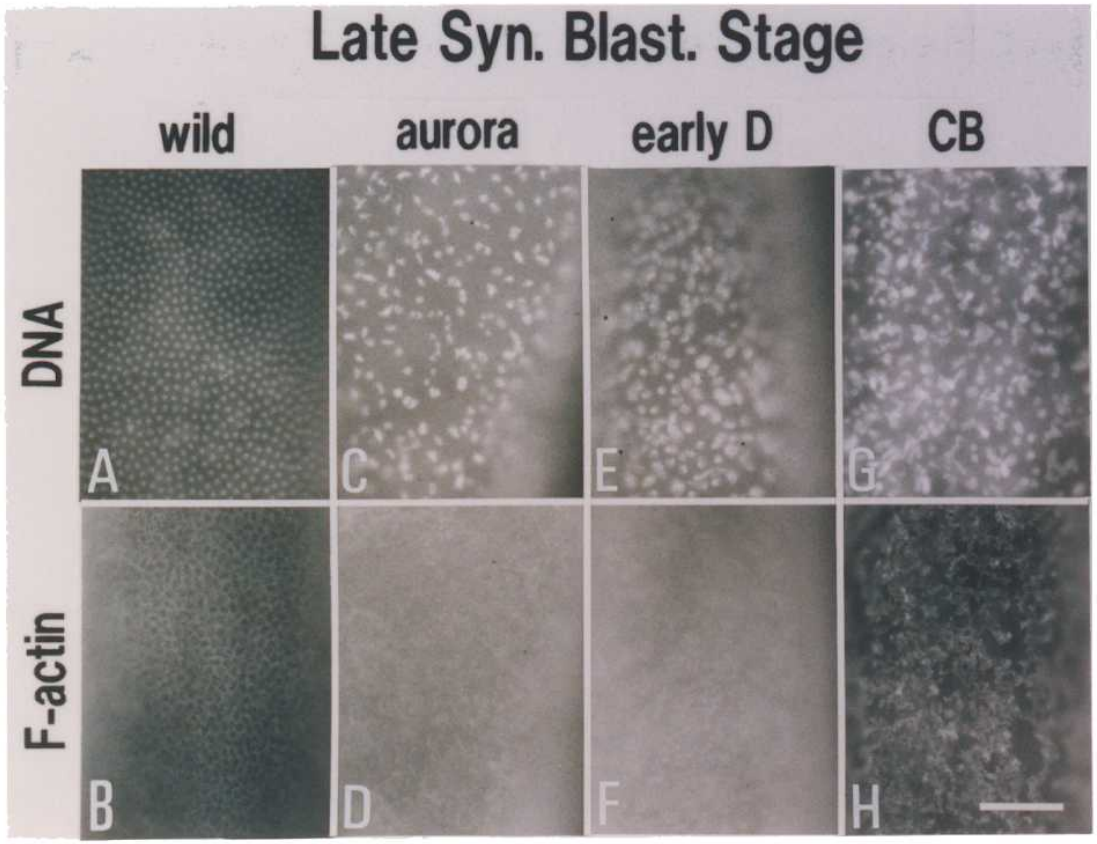
Late Syn. Blast. Stage
wild
aurora
early D
CB
DNA
F-actin
A
B
C
D
E
F
G
H

Fig. 32. Complementation test of N26 with deficiency strains. Solid lines represent the areas deleted in the respective deficiency strains that complemented N26. Bold lines represent the areas deleted in the respective deficiency strains that did not complement N26. The cytological map position of N26 was located in the region between broken lines. The drawing of a salivary grand chromosome in this figure is according to Lindsley and Grell (1986).

Cytological Mapping of N26

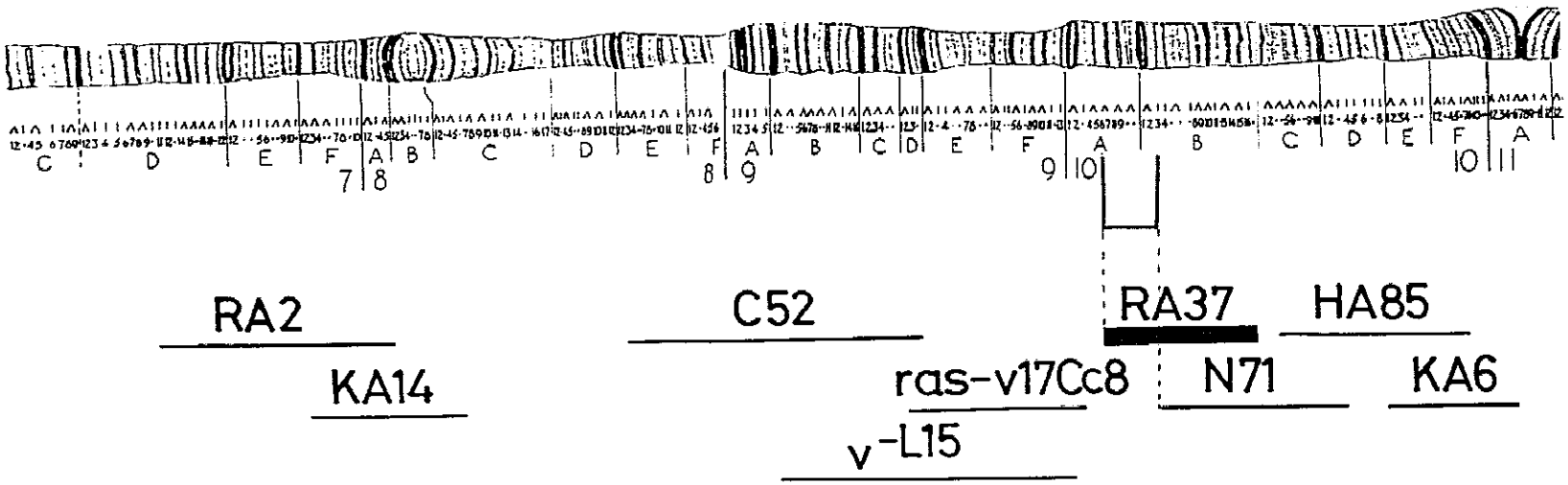

Fig. 33. Complementation test of N441 with deficiency strains. Solid lines represent the areas deleted in the respective deficiency strains that complemented N441. Bold lines represent the areas deleted in the respective deficiency strains that did not complement N441. The cytological map position of N441 was located in the region between broken lines. The drawing of a salivary grand chromosome in this figure is according to Lindsley and Grell (1986).

Cytological Mapping of N441

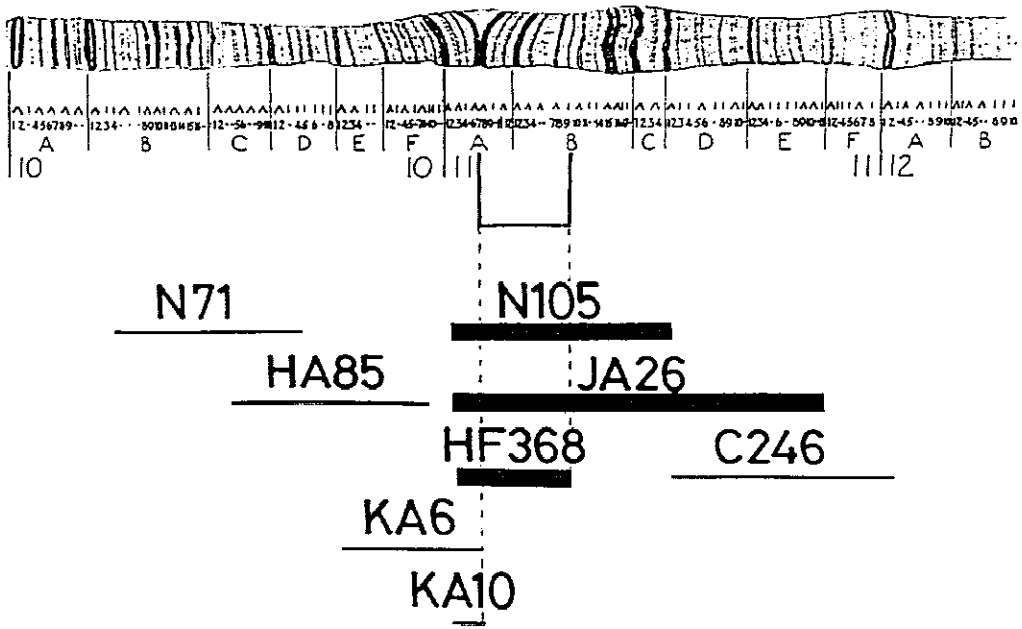

Fig. 34. Two-dimensional gel electrophoresis of ovarian proteins of the wild type (A), N441 (B) and N26 (C). Arrowhead (a) represents the spot of actin in each gel; arrows (b)-(e) represent the spots that show some differences in the positions or in the size among the strains.

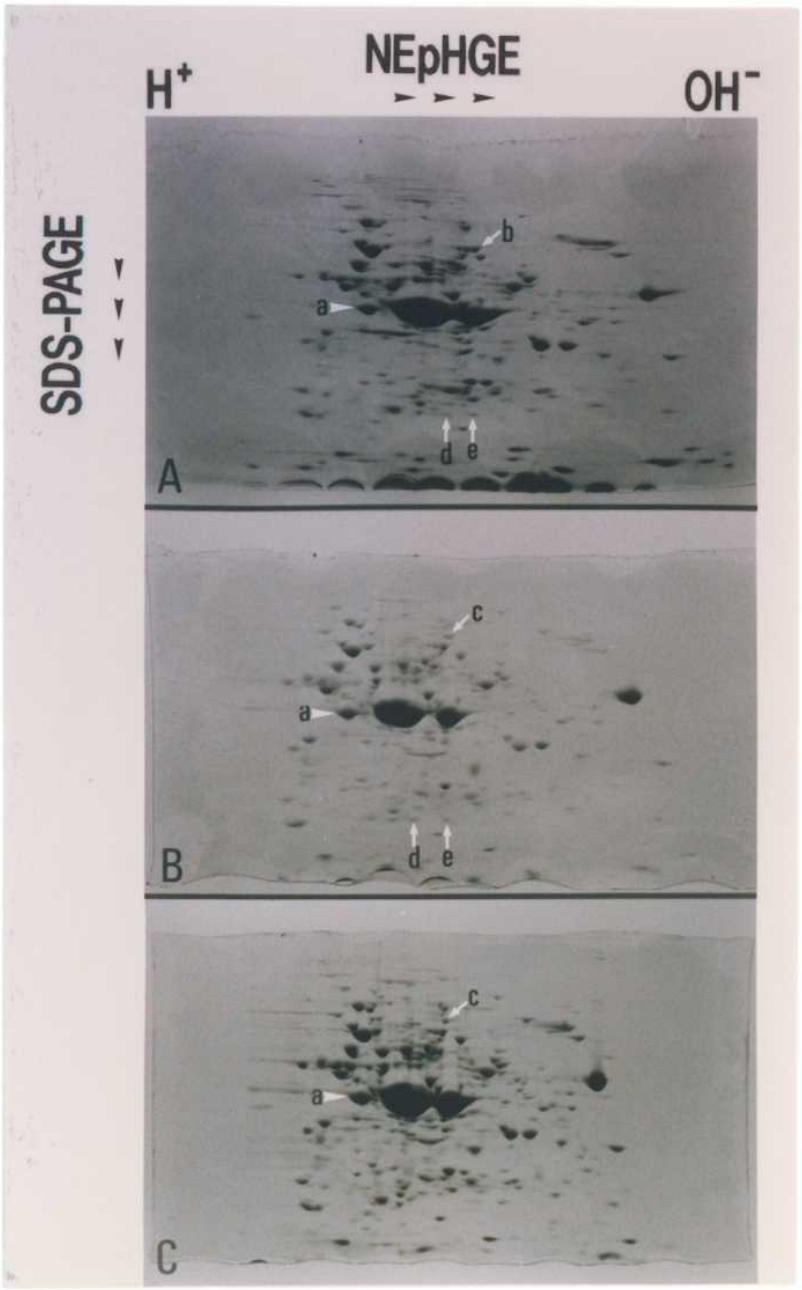
NEpHGE
H+
OH-
SDS-PAGE
A
B
C
a
b
c
d
e

Fig. 35. Change in the range of nuclear distribution along the anteroposterior axis throughout the cleavage stages in the embryos from N441/Df(1)N105 mothers raised under a restrictive condition (A) and a permissive condition (B). The positions of the most anterior and the most posterior nuclei are shown. Nuclei are distributed between solid lines in embryos from N441/N441 mothers and between broken lines in ones from N441/Df(1)N105 mothers. 0% egg length represents the posterior pole. Vertical bars represent standard errors.

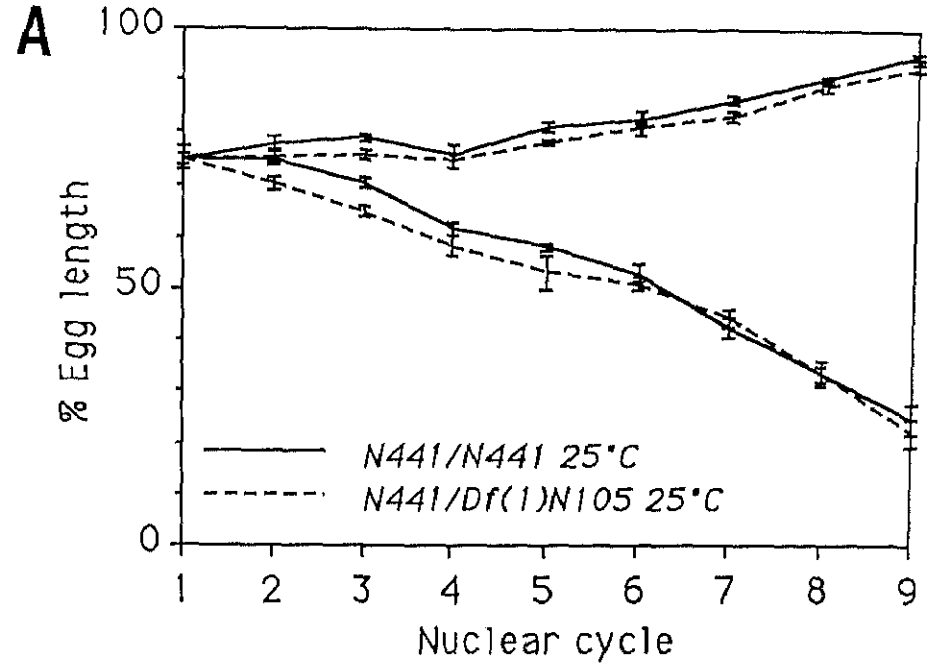
A
100
50
0
% Egg length
N441/N441 25°C
N441/Df(1)N105 25°C
1
2
3
4
5
6
7
8
9
Nuclear cycle

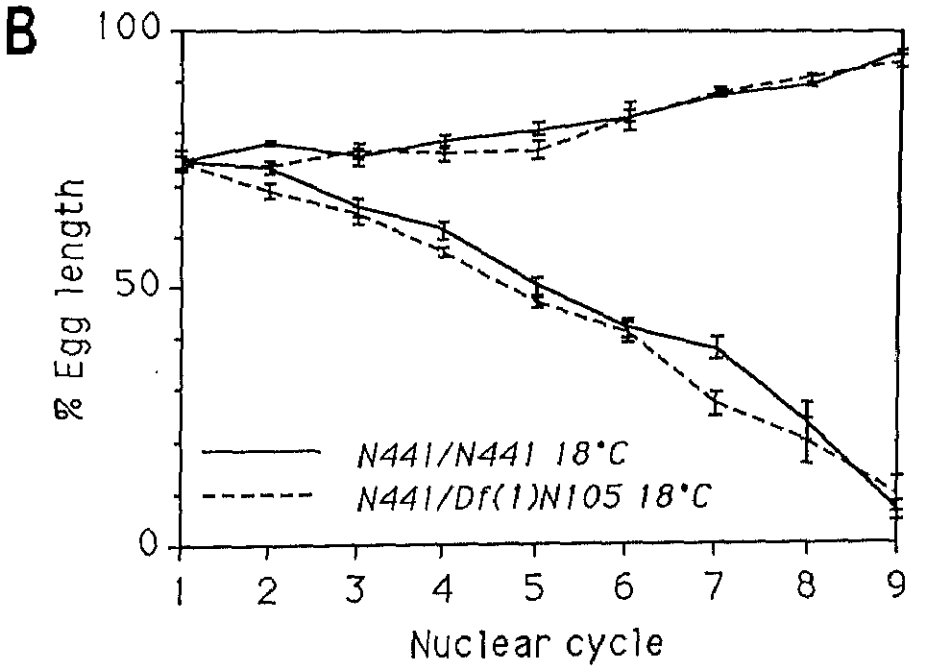
B
100
50
0
% Egg length
N441/N441 18°C
N441/Df(1)N105 18°C
1
2
3
4
5
6
7
8
9
Nuclear cycle

Fig. 36. Whole mount cycle-7 embryos from hemizygous mutant mothers raised under a restrictive condition. Nuclei were stained with DAPI. (A), a wild-type embryo; (B), an embryo from an N441/Df(1)N105 mother; (C), an embryo from a +/Df(1)RA37 mother; (D), an embryo from a par/Df(1)w^{258-45} mother. Bar represents 50 μm.

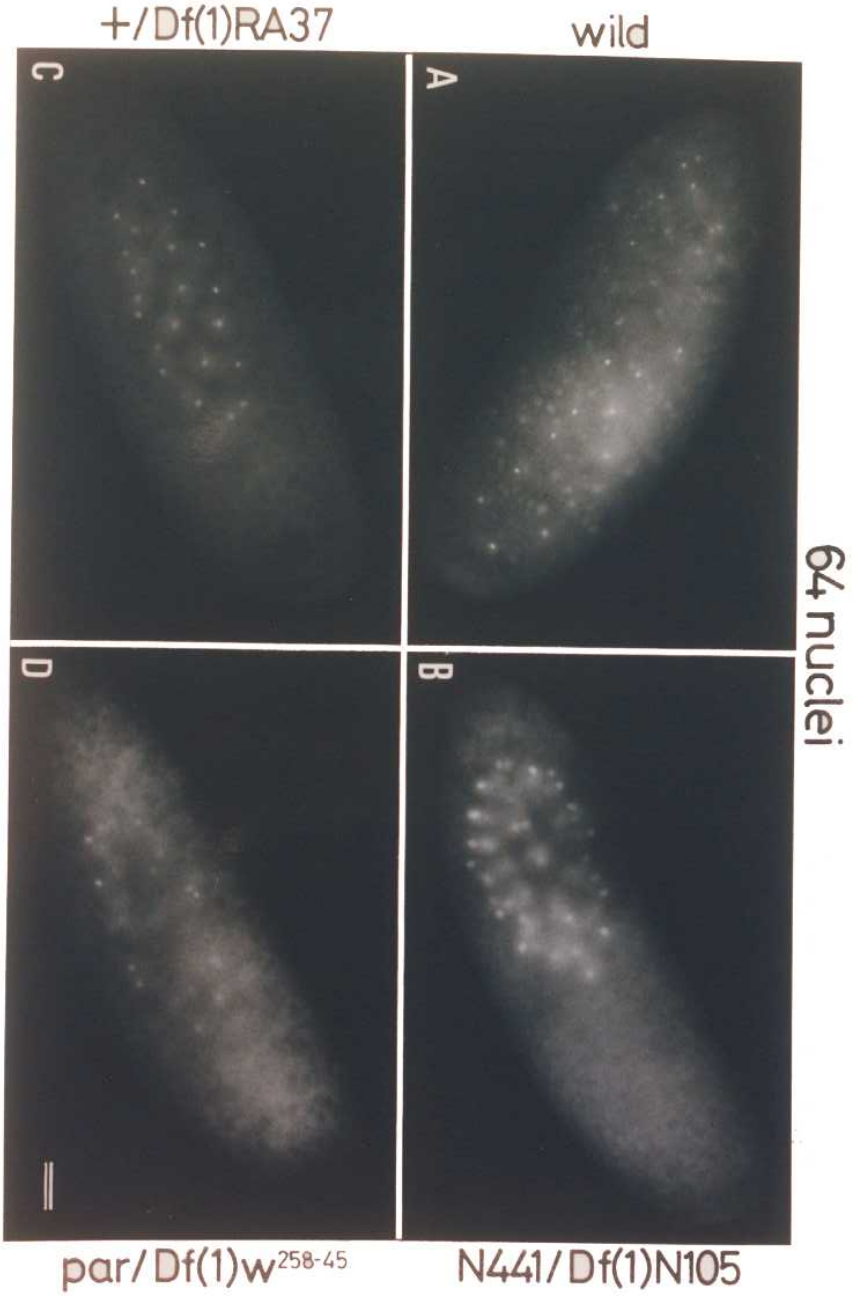
+/Df(1)RA37
wild
C
A
64 nuclei
D
B
par/Df(1)w258-45
N441/Df(1)N105

Fig. 37. The distribution of F-actin in the embryos shown in Figs. 36A-D, respectively. The embryos were stained with rhodaminyl phalloidin. Bar represents 50 μm.

64 nuclei

Fig. 38. The distributions of nuclei (A) and F-actin (B) in a cycle-7 embryo from a N26 N441/N26 N441 mother raised under a restrictive condition. The embryo was stained with DAPI in (A) and with rhodaminyl phalloidin in (B). Bar represents 50 μm.


A
B

Fig. 39. Fine structure of the posterior pole region of cycle-10 interphase (pole-bud stage) embryos. (A), a wild-type embryo; (B), a tud embryo. Arrowheads indicate polar granules and arrows indicate nuclear bodies. Bar represents 5 μm.

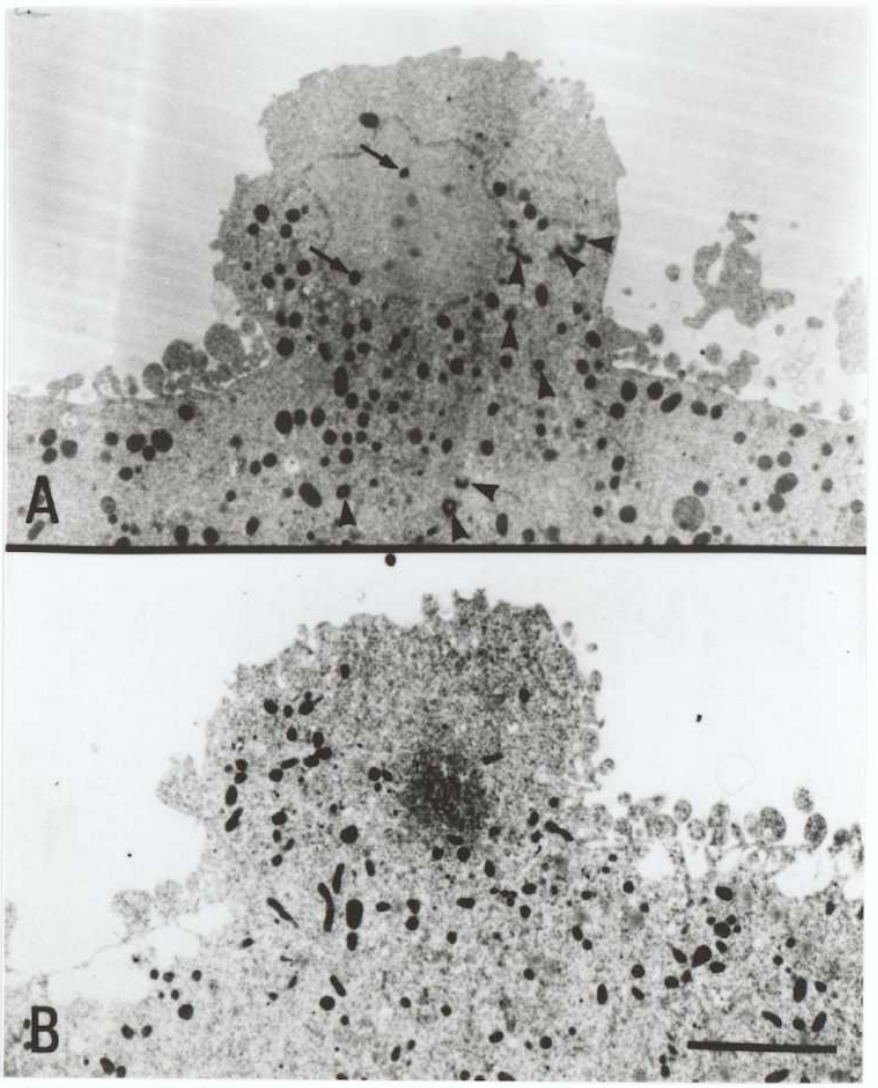
A
B

Fig. 40. Wild-type (A) and tud (B) embryos at cycle-9 interphase. The embryos were double-stained with DAPI and rhodaminyl phalloidin, and photographed on the same frame of film under respective excitation light by dual exposures. Arrowheads indicate nuclei showing blue staining. Orange or red color shows the stained F-actin. Bar represents 20 μm.

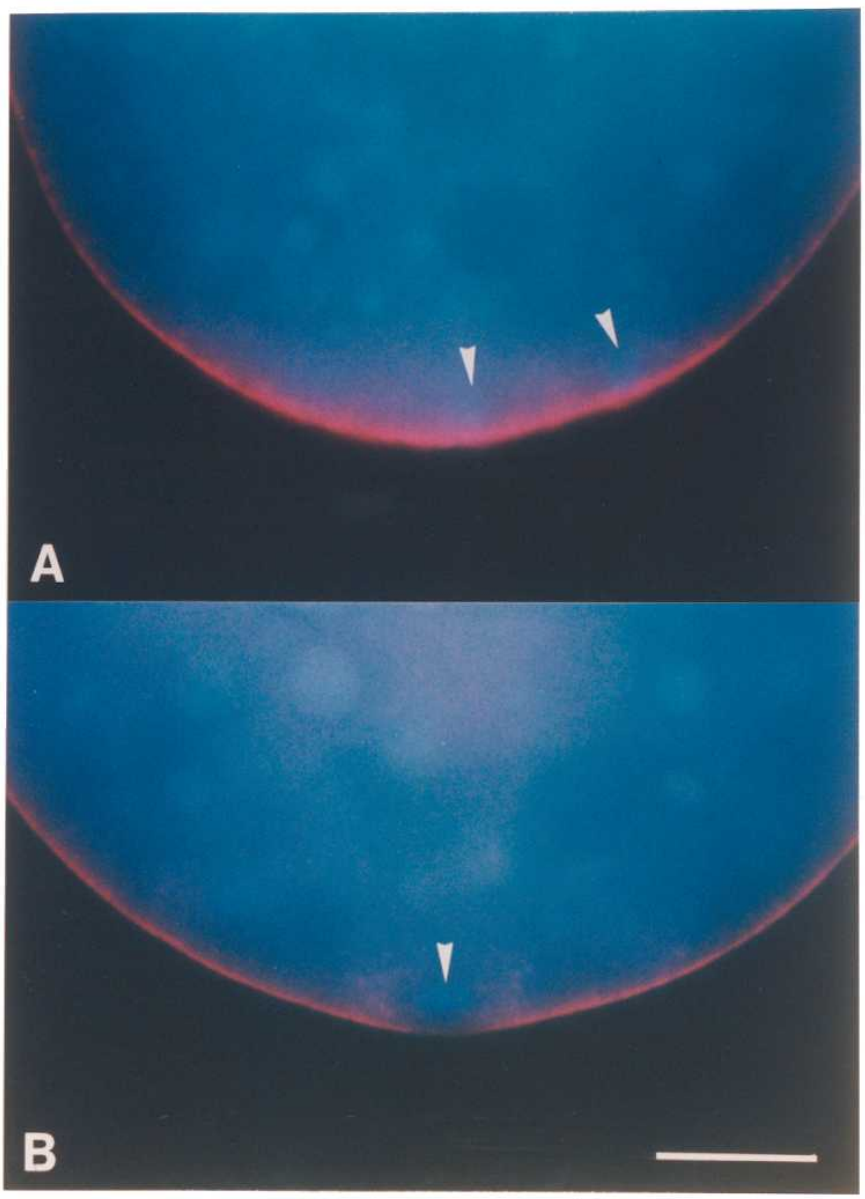
A
B

Fig. 41. Wild-type (A) and tud (B) embryos at cycle-10 prophase. The method for taking the photographs is the same as that described in the legend for Fig. 40. Bar represents 20 μm.

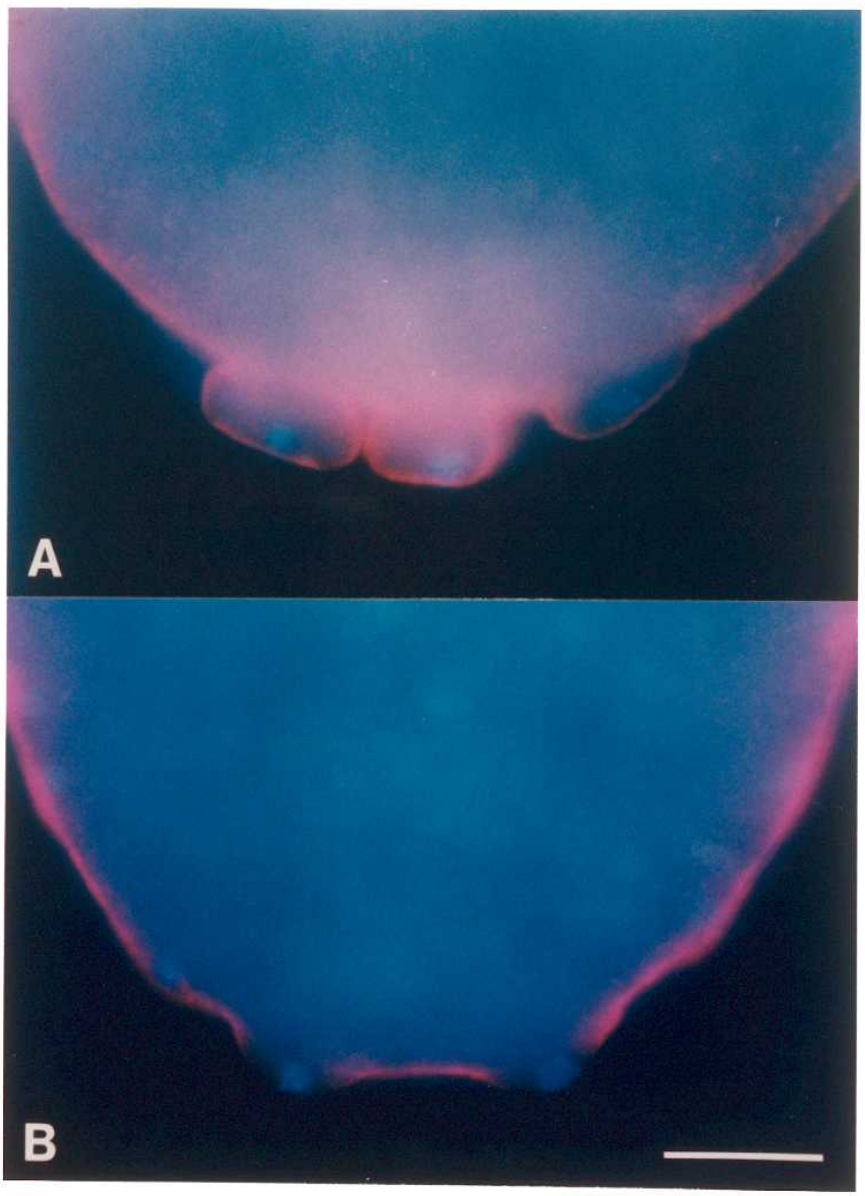
A
B

Fig. 42. Wild-type (A) and tud (B) embryos at cycle-10 metaphase. The method for taking the photographs is the same as that described in the legend for Fig. 40. Arrowhead indicates reduced fluorescence from cortical F-actin on the "pole bud" of the tud embryo. Bar represents 20 μm.

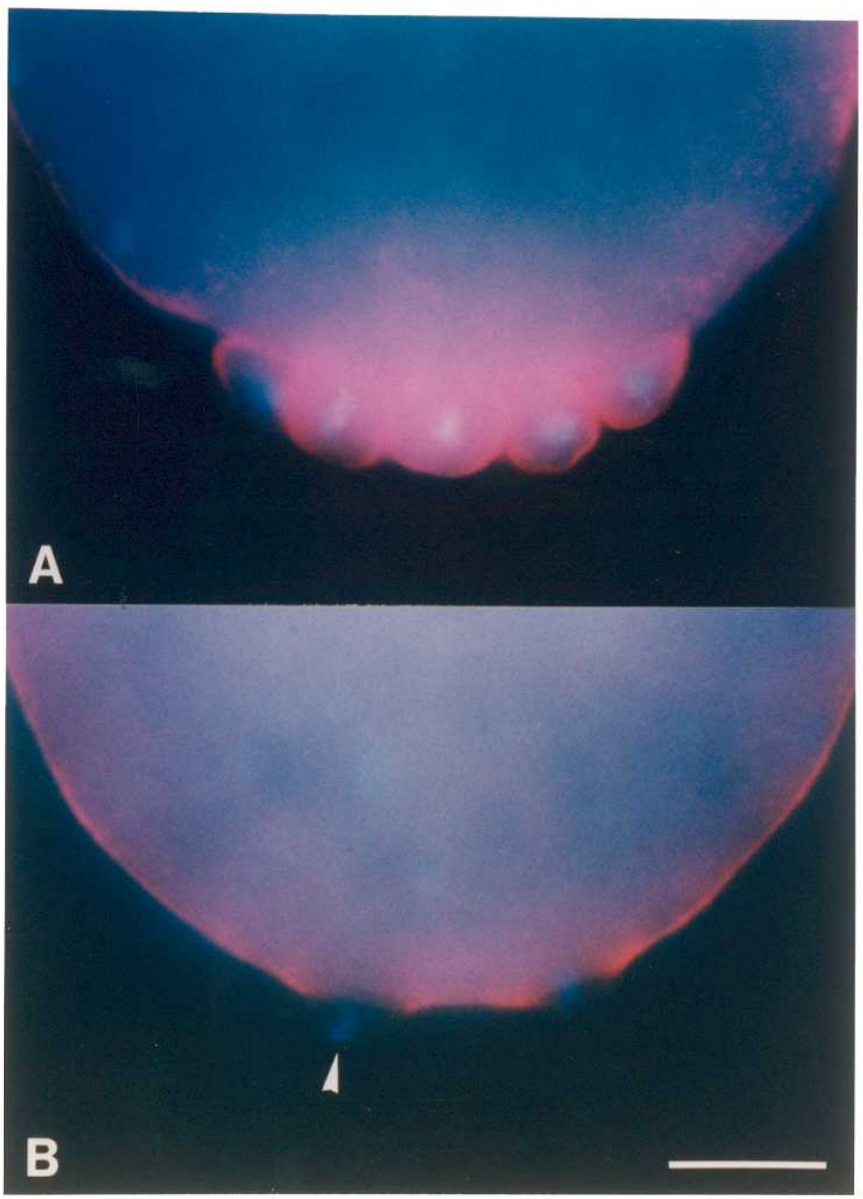
A
B

Fig. 43. Wild-type (A) and tud (B) embryos at cycle-10 telophase. The method for taking the photographs is the same as that described in the legend for Fig. 40. Bar represents 20 μm.

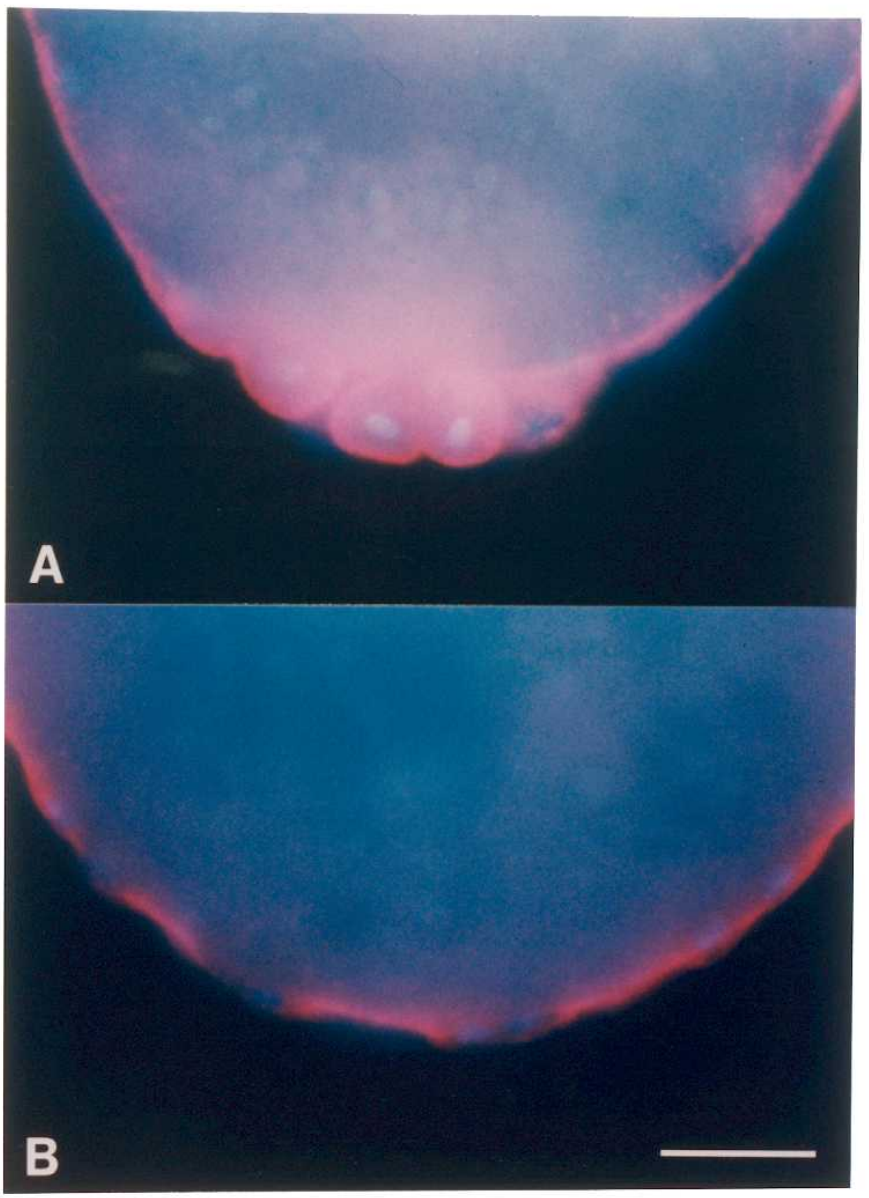
A
B

Fig. 44. Wild-type (A) and tud (B) embryos at cycle-14 late interphase (cellular blastoderm stage). The method for taking the photographs is the same as that described in the legend for Fig. 40. Arrowheads indicate pole cells, which are absent in the tud embryo (B). Bar represents 20 μm.

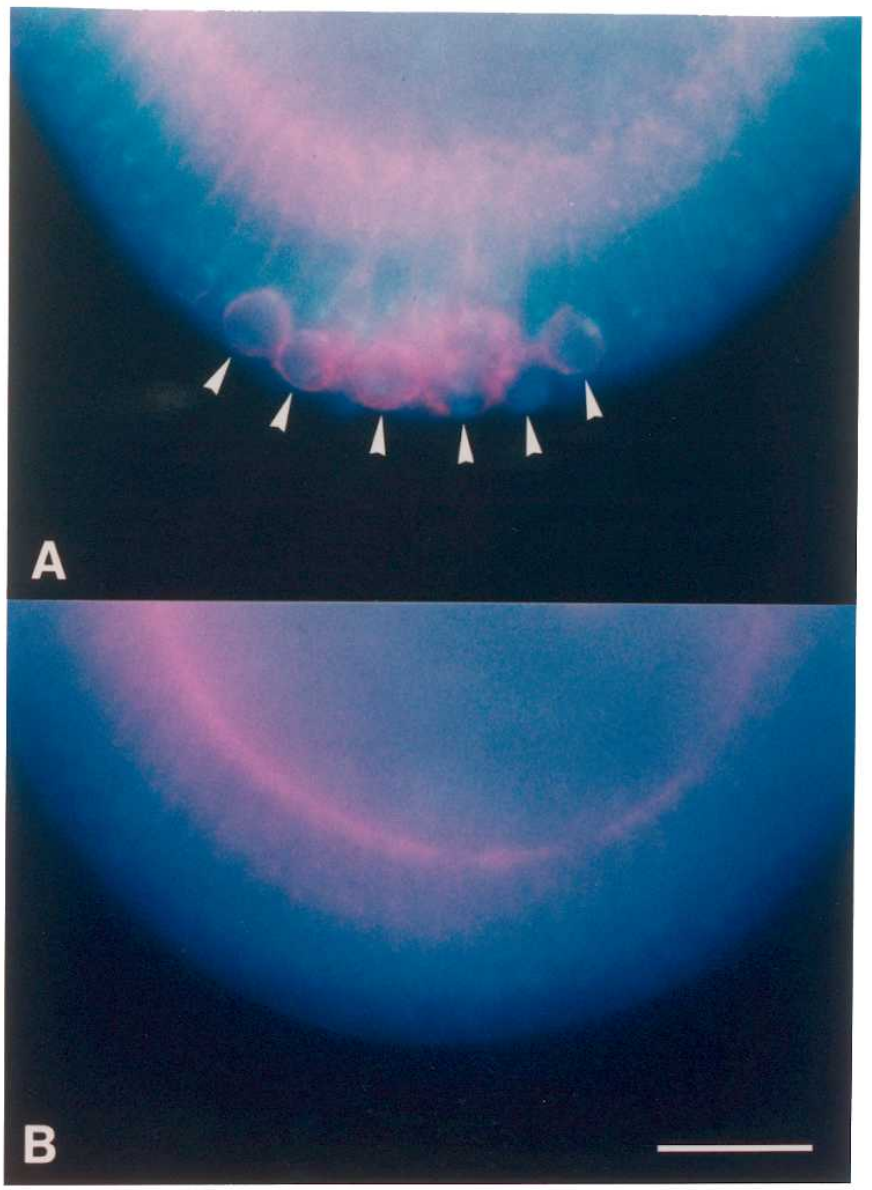
A
B